

# **Fungus-like mycelial fossils in 2.4 billion-year-old vesicular basalt**

Stefan Bengtson<sup>1\*</sup>, Birger Rasmussen<sup>2\*</sup>, Magnus Ivarsson<sup>1</sup>, Janet Muhling<sup>2,3</sup>, Curt Broman<sup>4</sup>, Federica Marone<sup>5</sup>, Marco Stampanoni<sup>5,6</sup> and Andrey Bekker<sup>7</sup>

<sup>1</sup>*Department of Palaeobiology and Nordic Center for Earth Evolution, Swedish Museum of Natural History, Stockholm, Sweden*

<sup>2</sup>*Department of Applied Geology, Curtin University, Bentley, WA, Australia*

<sup>3</sup>*School of Earth and Environment, The University of Western Australia, Perth, WA, Australia*

<sup>4</sup>*Department of Geological Sciences, Stockholm University, Stockholm, Sweden*

<sup>5</sup>*Swiss Light Source, Paul Scherrer Institute, Villigen, Switzerland*

<sup>6</sup>*Institute for Biomedical Engineering, University and ETH Zürich, Zürich, Switzerland*

<sup>7</sup>*Department of Earth Sciences, University of California, Riverside, CA, USA*

***Fungi have recently been found to comprise a significant part of the deep biosphere in oceanic sediments and crustal rocks. Fossils occupying fractures and pores in Phanerozoic volcanics indicate that this habitat is at least 400 million years old, but its origin may be considerably older. A 2.4 billion-year-old basalt from the Palaeoproterozoic Ongeluk Formation in South Africa contains filamentous fossils in vesicles and fractures. The filaments form mycelium-like***

*structures growing from a basal film attached to the internal rock surfaces. Filaments branch and anastomose, touch and entangle each other. They are indistinguishable from mycelial fossils found in similar deep-biosphere habitats in the Phanerozoic, where they are attributed to fungi on the basis of chemical and morphological similarities to living fungi. The Ongeluk fossils, however, are two to three times older than current age estimates of the fungal clade. Unless they represent an unknown branch of fungus-like organisms, the fossils imply that the fungal clade is considerably older than previously thought and that fungal origin and early evolution may lie in the oceanic deep biosphere rather than on land. The Ongeluk discovery suggests that life has inhabited submarine volcanics since more than 2.4 billions of years.*

The deep biosphere, hidden beneath land and sea, represents a major portion of life's habitats and biomass on Earth<sup>1</sup>. In spite of significant discoveries from scientific ocean drilling and metagenomics, the deep biosphere remains largely uncharted and its geological history almost entirely unknown. The deep habitats are protected from most of the hazards of surface life, and the deep environments would have been potentially available to life from the early stages of Earth's history. We report here filamentous structures preserved in carbonate- and chlorite-filled amygdales and fractures in basaltic lavas of the 2.4 Ga Ongeluk Formation, South Africa. Their morphology, dimensions, and striking similarity to fungi in Phanerozoic volcanics<sup>2-7</sup> indicate that they represent fossilized fungus-like mycelial organisms. The observation that fungus-like organisms inhabited submarine basaltic lavas more than 2.4 billion years ago suggests that this habitat was extremely conservative across the Proterozoic and Phanerozoic eons and raises questions about the antiquity of fungi and the early history of eukaryotes.

## 44 Geological setting

45 The Ongeluk Formation is a 900 m thick succession of basalts in the Griquatown West  
46 Basin, South Africa. The lavas are regionally extensive and comprise massive flows,  
47 pillow lavas and hyaloclastites that extruded onto the seafloor around 2.4 Ga; the basalts  
48 have undergone only very low-grade metamorphism (Supplementary Discussion). The  
49 fossiliferous sample (AG4) is a 25 cm long  $\frac{1}{4}$  core derived from drill depth 21.79–22.04  
50 m of the Agouron drillhole GTF01, which penetrated the lower part of the Ongeluk  
51 Formation (Fig. 1). About 70 of the ~100 observed amygdales contain filaments.

52 The sample is a chlorite-altered basalt with a relict igneous texture consisting of  
53 pseudomorphs of pyroxene and plagioclase (Supplementary Discussion). The  
54 groundmass consists of intergrown chlorite, K-feldspar, quartz, and calcite with  
55 accessory apatite and Fe-Ti oxides. Amygdales and veins are present, characterized by  
56 chlorite and calcite representing mineral infills of original vesicles and fractures in the  
57 lavas. The spherical to subspherical amygdales are up to 1.5 mm in diameter (Figs 2; 3).  
58 Most have rims composed of masses of very fine-grained, brownish green chlorite,  
59 Chlorite 1. Thermometry of Chlorite 1 yields metamorphic temperatures in the range of  
60 179–260°C (Supplementary Fig. 1; Supplementary Discussion). Where filaments are  
61 present, they are defined by Chlorite 1. No carbonaceous material has been detected  
62 within the filaments (Supplementary Fig. 2a). Calcite typically forms a cylindrical layer  
63 of constant thickness around the filaments; the blocky arrangement of crystals in the  
64 calcite, without clear relation to filament morphology (Fig. 4e), suggests that the calcite  
65 has been recrystallized. Fine-grained Chlorite 1 fills the space between the calcite  
66 cylinders (Figs 2b, d, e, g; 4; Supplementary Figs 3a, b; 4; 5). A second generation of

67 chlorite, Chlorite 2, coarser-grained and apple green, commonly intergrown with quartz  
68 and chalcopyrite, is present in some amygdales and fractures. Chlorite 2 is not pervasive  
69 but overprints Chlorite 1, including filaments defined by Chlorite 1 (Fig. 4d, e;  
70 Supplementary Fig. 4d). Thermometry of Chlorite 2 gives metamorphic temperatures of  
71 319–411°C (Supplementary Figs 1; 5; Supplementary Discussion). Its association with  
72 chalcopyrite, occurrence in veins, and otherwise non-pervasive distribution suggest that  
73 the growth of Chlorite 2 was linked to hydrothermal fluids.

#### 74 Filament structure and morphology

75 The filaments extend from rims of Chlorite 1 attached to amygdale and fracture walls  
76 and form a tangled network inside vesicles and fractures in the rock (Figs 2; 3; 4;  
77 Supplementary Fig. 3). The density of the filamentous network typically decreases  
78 toward the centre of the cavities (Figs 2b, d, j, 3a, e; 4b; Supplementary Fig. 3a, b). The  
79 chlorite rim represents an uneven basal film consisting of a jumbled mass with little  
80 space remaining between filaments (Figs 2j, k; 3e; Supplementary Fig. 3).

81 SEM/BSE/WDS images confirm that the structure and composition are identical  
82 between filaments and basal film (Fig. 2j, k; Supplementary Figs 4; 5).

83 Filaments are 2–12  $\mu\text{m}$  wide; the width is usually constant within a filament. No  
84 internal septa have been identified, but original internal structure is not preserved (Fig.  
85 2k, l). The filaments typically form straight or curved sections, rarely with irregular  
86 wiggly parts. Filaments frequently form loops of different diameter, from about 10  $\mu\text{m}$   
87 (Fig. 3h) to 80  $\mu\text{m}$  or more (Fig. 3i).

88 Branchings at acute angles, Y-junctions, are common among the free filaments (Figs 2c;  
89 3f, g). T-junctions also occur (Fig. 3g), though considerably less frequently. Filaments

90 with different orientation commonly touch and entangle each other (Fig. 3f, i), and  
91 crossing filaments sometimes seem to merge seamlessly. Where none of the filaments  
92 change direction the crossing is interpreted as coincidental (Fig. 2l). This phenomenon  
93 of taphonomic/diagenetic filament merging makes it sometimes difficult to identify true  
94 branching, where a single filament is split into two. When Y-junctions on the same  
95 apparently branching filament point in opposite directions (Fig. 3c), one or both  
96 junctions may represent false branching; this can also be indicated by the filament being  
97 thicker, or even appearing doubled, below a Y-junction. There are, however, a number  
98 of cases where the morphology of the junction leaves little doubt of true branching (Figs  
99 2c; 3f, g). In particular, where successive Y-branching takes place from a stem of  
100 constant diameter, the branching is real and not due to bundling of separate filaments  
101 (Fig. 3f, g).

102 Anastomoses, where a branched-off filament meets and merges with another, occur with  
103 some frequency (Figs 2c, f; 3b, c). As with branching, it may be difficult to distinguish  
104 coincidental coming-together of independent filaments from true anastomoses, but the  
105 frequency of apparent anastomoses with consistent morphology (e.g., Fig. 3b, c)  
106 indicates that the phenomenon is real. Nonetheless, anastomoses do not dominate the  
107 filament tangles to the extent that they form interlocking networks.

108 The filaments sometimes carry bulbous protrusions, 5–10  $\mu\text{m}$  in diameter. These tend to  
109 congregate on the basal parts of filaments and on basal films, and be more rare on distal  
110 parts of filaments (Fig. 3j).

111 A recurring feature is a bundle of filaments giving off diverging branches to form a  
112 broom-like structure, here termed “broom”, that extends from the basal film or from the

113 substrate (Figs 2e, g, h; 3d, e). In some vesicles there are brooms consisting of tens of  
114 diverging filaments, some with their bases apparently attached to the vesicle wall and  
115 some produced by branching (Supplementary Fig. 3c, d).

116 The basalt is permeated by veins that are frequently seen to connect to the  
117 spherical/subspherical vesicles (Fig. 2a, i; Supplementary Video). The veins, down to 5  
118  $\mu\text{m}$  in width, are filled with chlorite and calcite similar to that, which fills the vesicles.  
119 One large vein, >2.2 mm long and >0.2 mm wide, comprises a zone of densely  
120 intertwined filaments that occurs between the basalt wall-rock and the centre of the  
121 vein. Filaments adjacent to the margin of the vein are commonly truncated by chlorite  
122 sheets and veinlets (Fig. 4) representing a later stage of chlorite growth (Chlorite 2;  
123 Supplementary Discussion).

#### 124 Biogenicity and syngenicity

125 Crucial to the interpretation of the filaments are the issues of biogenicity and  
126 syngenicity: Do the filaments represent biological organisms and when did they form  
127 relative to the age of the rock? Filamentous fabrics are not uncommon in basaltic rocks,  
128 though most reported cases refer to tunnelling in volcanic glass and its alteration  
129 products<sup>8</sup>. Both biogenic and abiogenic mechanisms may be responsible for such  
130 tunnels, and distinguishing between the two causes is difficult and controversial<sup>9-12</sup>. A  
131 number of observations clearly indicate, however, that the Ongeluk structures were  
132 formed as filaments in voids, not as tunnels in minerals:

133 (1) Although tunnels may take on a variety of shapes, including branching and dendritic  
134 ones<sup>13</sup>, several features of the Ongeluk structures are incompatible with tunnels. The  
135 frequent fusing of adjacent filaments (Fig. 3f, i), resulting in false branching (Fig. 3c),

136 implies that the filaments are physical entities frequently touching and entangling each  
137 other. This is consistent with flexible filaments in a void but not with tunnelling in rock.  
138 Similarly, the recurring cases of anastomosis (Figs 2 and 3) are difficult to reconcile  
139 with tunnels.

140 (2) The morphology of the filaments and the mineral paragenetic sequence in the  
141 fractures (Fig. 4) are identical to those of the adjacent vesicles, implying that the  
142 vesicles, like the fractures, started out as voids and underwent the same history of  
143 colonization and paragenesis.

144 (3) A number of different spherical or globular structures are found in volcanic and  
145 subvolcanic rocks<sup>14</sup>. They may be formed as gas bubbles in the magma (vesicles), as  
146 radial growth of crystals (spherulites), or as the result of immiscibility of component  
147 magmatic fluids (varioles). Vesicles usually become filled by secondary minerals  
148 formed at low temperatures, forming amygdalites. The Ongeluk spherical structures are  
149 filled with minerals (mainly calcite and chlorite) characteristic of amygdalites; they show  
150 neither spherulitic structure nor magmatic composition, and so may confidently be  
151 interpreted as having begun as gas bubbles (Supplementary Discussion).

152 (4) The Ongeluk filaments fulfil established criteria<sup>15</sup> distinguishing cryptoendoliths  
153 (cavity-dwellers) and chasmoendoliths (fracture-dwellers) from euendoliths (rock-  
154 borers) and abiotic processes forming microtunnels in rock (Supplementary Discussion).  
155 They show pre-metamorphic growth into fluid-filled cavities, curvilinear and branching  
156 forms with circular cross-section and non-uniform diameter, and preservation in clays  
157 with or without organic matter in carbonate-filled vesicles; all listed as characters  
158 typical of crypto- and chasmoendoliths<sup>15</sup>.

159 Lepot et al.<sup>16</sup> reported a variety of structures interpreted as ambient inclusion trails in an  
160 Archaean pyroclastic tuff. Their “Type 1 microtubes” show a compositional similarity  
161 with the Ongeluk structures: both have chloritic cores surrounded by calcite. They differ  
162 from the latter, however, in being straight and very regular.

163 A commonly stated criterion for biogenicity of microfossils is the presence of original  
164 organic carbon in the structures; this has even been cited as a necessary criterion<sup>12,17</sup>.  
165 However, organic carbon is seldom preserved in environments of highly oxidized  
166 minerals, such as calcite or hematite; organically preserved microfossils are  
167 predominantly found under preservational conditions of low permeability and reactivity,  
168 as in cherts<sup>18</sup>. Because the absence of organic carbon in a fossil is seldom reported in  
169 the literature, the lack of such carbon is frequently overlooked. It is, however, a  
170 common condition<sup>18</sup>. For example, we have investigated well-preserved iron-oxidizing  
171 bacteria in a Quaternary microbialite where filaments are encrusted with hematite, and  
172 Raman spectroscopy failed to reveal any organic carbon signal<sup>19</sup>. The lack of detectable  
173 carbonaceous matter in the Ongeluk filaments is thus not a valid argument against their  
174 biogenicity.

175 With regard to syngenicity, the organisms must have invaded the Ongeluk lavas while  
176 the vesicles and fracture-controlled porosity were still open to the water column, a  
177 window that likely closed after ca 10 million years following the eruption of the lavas<sup>20</sup>.  
178 In any case they should not be younger than ca. 2.06 Ga, at which time chloritization  
179 would have taken place (Supplementary Discussion). Supplementary Fig. 6 depicts the  
180 proposed formation sequence from invasion of the organism through diagenesis and  
181 metamorphism.

182 Raman spectroscopy indicates the presence in the Ongeluk host basalt of carbonaceous  
183 material (CM) that has not been subject to higher temperatures than about  $200\pm 30^{\circ}\text{C}$ ;  
184 CM in the Ongeluk basal sandstone and the underlying Makganyene diamictite yields  
185 temperatures around  $370^{\circ}\text{C}$  (Supplementary Fig. 7; Supplementary Discussion). The  
186 origin of the carbon is unknown; it shows no affinity to the filaments (Supplementary  
187 Fig. 2).

## 188 Biology of the filaments

189 Filamentous growth is a recurring characteristic in many multicellular prokaryotes and  
190 algae, but mycelial networks consisting of branching filaments are known mainly from  
191 three modern groups of organisms, actinobacteria, fungi, and the fungus-like eukaryotic  
192 oomycetes. Mycelium-forming actinobacteria produce radiating networks of branching  
193 filaments,  $0.15\text{--}1.5\text{ }\mu\text{m}$  in diameter. Anastomoses are generally absent<sup>21</sup>; occasional  
194 reports of anastomoses in *Streptomyces* have not been confirmed<sup>22</sup>. Many actinobacteria  
195 form spores, about  $1\text{ }\mu\text{m}$  in diameter, on the mycelium, sometimes in sporangia  $5\text{--}20$   
196  $\mu\text{m}$  in size<sup>23</sup>. Actinobacteria have a wide distribution in aquatic and terrestrial habitats,  
197 including various extreme environments<sup>24</sup>.

198 Like actinobacteria, fungi are widely distributed in terrestrial and aquatic habitats, and  
199 they have recently been shown to be common inhabitants of deep-marine sediments and  
200 crustal rocks<sup>5,25-29</sup>. Hyphae in fungal mycelia vary in width between  $2$  and  $27\text{ }\mu\text{m}$ <sup>30</sup>.  
201 Anastomoses are prevalent<sup>31</sup>, and the mycelia typically form networks of interconnected  
202 hyphae. Fungal spores are larger than those of actinobacteria, typically around  $5\text{ }\mu\text{m}$ .

203 Fungi have recently been found to play a leading role in the Phanerozoic subsurface  
204 biota through the discoveries of fossilized fungal mycelia in vesicles in Devonian,

205 Eocene and Quaternary submarine volcanics<sup>2-7,28</sup>. These fungi may form symbiotic  
 206 assemblages with prokaryotes<sup>32,33</sup>.

207 The oomycetes were previously thought to be fungi, but molecular systematics now  
 208 places them close to the photosynthetic stramenopiles<sup>34</sup>. Anastomoses between hyphae  
 209 occasionally occur, but as a form of conjugation, not a mechanism to form interlocking  
 210 networks<sup>35</sup>.

211 When compared with modern mycelial organisms, the Ongeluk fossils in hyphal  
 212 dimensions, network architecture, and mode of life seem most consistent with fungi. If  
 213 the 5–10 µm bulbous protrusions are spores, those too agree with fungal but not  
 214 actinobacterial dimensions. Ongeluk anastomoses closely mimic those in modern fungi  
 215 (compare Figs 2c, f and 3b, c herein with anastomoses figured by Sbrana et al.<sup>36</sup>, fig. 1).  
 216 Other features of the Ongeluk fossils, such as the basal film and the tendency of  
 217 filaments to protrude from the basal film as brooms, are consistent with fungal mycelial  
 218 morphology (e.g., the mycelial cords developed by many fungi under conditions of  
 219 starvation<sup>37</sup>). The growth habit of the Ongeluk filaments in basaltic vesicles is  
 220 morphologically almost identical to that seen in fungi in Phanerozoic volcanics  
 221 (Supplementary Fig. 8)<sup>2-7,32,33</sup>. The examples from Devonian pillow lavas<sup>3,4</sup> are  
 222 particularly significant because they show preservational features similar to those in the  
 223 Ongeluk vesicles, with mineral encrustations of the filaments (Supplementary Fig. 8a–  
 224 d). In the Devonian occurrences, however, the encrusting minerals include illite and  
 225 glauconite as well as chamosite (chlorite).

226 Although on the basis of morphology we cannot exclude the possibility that the  
 227 Ongeluk fossils represent a separate branch of fungus-like organisms, the similarities

228 with fungi in the corresponding Phanerozoic settings are striking. The presence of fungi  
229 in early Palaeoproterozoic submarine volcanic rocks would, however, overturn current  
230 concepts on the timing and circumstances of fungal origin and evolution. There is a  
231 strong consensus that fungi and nucleariids comprise the sister group of holozoans  
232 within the clade Opisthokonta<sup>38-40</sup>, and the time of divergence of the two sister branches  
233 is commonly estimated to lie within the Mesoproterozoic or earliest Neoproterozoic<sup>41-47</sup>.  
234 The last common ancestor of crown-group fungi is considered to have been non-  
235 filamentous, with flagellated spores, aquatic, but probably non-marine<sup>39</sup>. Under this  
236 scenario, marine and deep-biosphere fungi might represent migrated terrestrial taxa,  
237 consistent with the predominance in marine and deep-biosphere environments of  
238 advanced forms<sup>5,7,26,27,29,48</sup>. Fungi living in submarine basalts at 2.4 Ga, however, would  
239 imply that the fungal clade is considerably older than previously thought and that fungal  
240 origin and early evolution may lie in the oceanic deep biosphere rather than on land.

241 Estimates of node ages from molecular clocks rely on calibration against the fossil  
242 record. Whereas the Phanerozoic fossil record is sufficiently reliable to yield useful  
243 calibration points<sup>49</sup>, the Proterozoic record is notoriously spotty, and interpretations of  
244 Proterozoic fossils are frequently controversial (e.g., alleged Proterozoic fungi<sup>46</sup>). Ages  
245 of Proterozoic nodes are therefore typically based on extrapolations from Phanerozoic  
246 calibration points. Irrespective of the formidable molecular-clock problems, the  
247 existence of fungi near the beginning of the Proterozoic, before or at the very early stage  
248 of the Great Oxidation Event, would raise issues about the existence of other major  
249 eukaryote branches at the time.

250 Whether or not the Palaeoproterozoic Ongeluk fossils represent fungi, the occurrence of  
251 remarkably similar fossils in Phanerozoic vesicular basalts (Supplementary Fig. 8)<sup>2-7,32</sup>  
252 suggests that this environment has been extremely stable over billions of years. Locally  
253 and regionally an environment such as that provided by the Ongeluk lavas may be short-  
254 lived, however, and whether colonizing biota under such conditions was preferentially  
255 supplied from the seawater or from the subsurface environments is an open question.  
256 The taxonomic characterization of cavity-dwelling mycelial organisms over time will  
257 help to answer the question of the spatial and temporal diversity and evolution of the  
258 deep biosphere.

## 259 Material and methods

260 The sample was cut to produce 14 petrographic thin sections and 7 pillars, 2 mm wide.  
261 The sections were studied using optical microscopy and scanning electron microscopy  
262 (SEM/ESEM) as well as synchrotron-radiation X-ray tomographic microscopy  
263 (SRXTM).

### 264 Environmental scanning electron microscopy

265 The images in Fig. 2j–l were obtained with a Philips XL30 environmental scanning  
266 electron microscope (ESEM) with a field emission gun (XL30 ESEM-FEG) and a vCD  
267 backscatter electron detector. The acceleration voltage was 20 kV. The samples were  
268 not coated.

### 269 X-ray microanalysis

270 Chlorite and carbonate (calcite) within the amygdales were analysed with an Oxford  
271 Instruments X-Max50 EDS mounted on a TESCAN VEGA3 scanning electron

272 microscope (SEM). Aztec software was used to collect and process the X-ray spectra  
273 from carbon-coated thin sections. Fully quantitative data were collected at 15 kV  
274 accelerating voltage and 1–2 nA beam current. The system count rate was calibrated  
275 using pure copper, and standard spectra were collected on the VEGA3 from jadeite  
276 (Na), periclase (Mg), corundum (Al), wollastonite (Si and Ca), orthoclase (K), rutile  
277 (Ti), chromite (Cr), rhodonite (Mn) and pyrite (Fe). Analytical precision is  $\pm 1$ –2%  
278 relative for major elements ( $>10$  wt%) and  $\pm 5$ –10% relative for minor elements ( $<10$   
279 wt%). Twenty-five point analyses from Chlorite 1 and 25 point analyses from Chlorite 2  
280 were collected at 15 kV and 20 nA using a JEOL 8530F electron microprobe fitted with  
281 five wavelength dispersive X-ray spectrometers (WDS). Quantitative analyses were  
282 derived using Probe for EPMA from Probe Software, Inc. Standards used were jadeite  
283 (Na), periclase (Mg), corundum (Al), wollastonite (Si and Ca), orthoclase (K), rutile  
284 (Ti),  $\text{Cr}_2\text{O}_3$  (Cr), spessartine (Mn) and magnetite (Fe). Analytical precision is  $\pm 1$ %  
285 relative for major elements ( $>10$  wt%) and  $\pm 5$ –10% relative for minor elements ( $<10$   
286 wt%).

## 287 Element distribution maps

288 Quantitative element distribution maps of amygdales from thin section ZBF061 were  
289 generated using an FEI Verios XHR SEM, operating with 15 kV accelerating voltage  
290 and approximately 1–2 nA beam current. X-ray maps were collected and processed  
291 using an Oxford Instruments X-Max80 Energy Dispersive X-ray detector (EDS) and  
292 Aztec software. The section was coated with a 20 nm thick carbon film before analysis.  
293 Element distribution maps for temperature mapping were collected from part of an  
294 amygdale from thin section ZBF061 with the JEOL 8530F at 15 kV accelerating voltage

295 and 50 nA beam current. The maps were collected and processed (deadtime,  
296 background and overlap corrections) using Probe for EPMA software from Probe  
297 Software, Inc. The corrected data were read into XMapTools<sup>51</sup> where they were  
298 calibrated using the WDS point analyses and converted into quantitative maps of the  
299 element oxides. Pixel by pixel (1  $\mu\text{m}$  x 1  $\mu\text{m}$ ) temperature estimates, based on the  
300 calibration of Bourdelle et al.<sup>52</sup>, were made in XMapTools and plotted as a temperature  
301 map.

## 302 Raman spectrometry

303 Raman spectra were collected using a confocal laser Raman microspectrometer (Horiba  
304 instrument LabRAM HR 800; Horiba Jobin Yvon, Villeneuve d'Ascq, France),  
305 equipped with a multichannel air-cooled ( $-70^{\circ}\text{C}$ ) 1024 x 256 pixel CCD (charge-  
306 coupled device) detector at the Department of Geological Sciences, Stockholm  
307 University. Acquisitions were obtained with an 1800 lines/mm grating. Excitation was  
308 provided by an Ar-ion laser ( $\lambda=514$  nm) source. Spectra were recorded using a low laser  
309 power of 0.1–1 mW at the sample surface to avoid laser-induced degradation of the  
310 samples. Sampling was carried out using an Olympus BX41 microscope coupled to the  
311 instrument, and the laser beam was focused through a 100x objective to obtain a spot  
312 size of about 1  $\mu\text{m}$ . The spectral resolution was  $\sim 0.3$   $\text{cm}^{-1}$ /pixel. The typical exposure  
313 time was 10 s with 10 accumulations. The accuracy of the instrument was controlled by  
314 repeated use of a silicon wafer calibration standard with a characteristic Raman line at  
315  $520.7$   $\text{cm}^{-1}$ . Instrument control and data acquisition were made with LabSpec 5  
316 software.

317 Tomographic microscopy

318 Synchrotron-radiation tomographic microscopy was carried out at the TOMCAT  
319 beamline of the Swiss Light Source at the Paul Scherrer Institute, Villigen, Switzerland.  
320 X-ray energy was set to 15 keV for petrographic thin sections and 28 keV for sawn-out  
321 2 mm pillars. Objectives x4, x10 and x20 were used, for a voxel size of 1.625  $\mu\text{m}$ , 0.65  
322  $\mu\text{m}$  and 0.325  $\mu\text{m}$ , respectively. Pillars were first scanned in total at low magnification  
323 to identify fossiliferous vesicles later to be scanned at higher magnifications. For the  
324 results presented here, 1501 projections were acquired equiangularly over 180°, online  
325 post-processed and rearranged into flat- and darkfield-corrected sinograms.  
326 Reconstruction was performed on a Linux PC farm using highly optimized routines  
327 based on the Fourier Transform method<sup>53</sup>. Slice data derived from the scans were  
328 analyzed and rendered using Avizo software.

329 **Data Availability Statement.** The illustrated material is deposited at the Swedish  
330 Museum of Natural History, Stockholm. The datasets generated and/or analysed during  
331 the current study are available from the corresponding author on request.

332 **Supplementary Information** is linked to the online version of the paper at  
333 [www.nature.com/nature](http://www.nature.com/nature).

## 334 References

- 335 1 Edwards, K. J., Becker, K. & Colwell, F. The deep, dark energy biosphere:  
336 intraterrestrial life on Earth. *Annu Rev Earth Planet Sci* **40**, 551–568 (2012).
- 337 2 Schumann, G., Manz, W., Reitner, J. & Lustrino, M. Ancient fungal life in  
338 North Pacific Eocene oceanic crust. *Geomicrobiol. J.* **21**, 241–246 (2004).

339 3 Peckmann, J., Bach, W., Behrens, K. & Reitner, J. Putative cryptoendolithic life  
340 in Devonian pillow basalt, Rheinisches Schiefergebirge, Germany. *Geobiology* **6**, 125–  
341 135 (2008).

342 4 Eickmann, B., Bach, W., Kiel, S., Reitner, J. & Peckmann, J. Evidence for  
343 cryptoendolithic life in Devonian pillow basalts of Variscan orogens, Germany.  
344 *Palaeogeogr., Palaeoclimatol., Palaeoecol.* **283**, 120–125 (2009).

345 5 Ivarsson, M. *et al.* Fossilized fungi in subseafloor Eocene basalts. *Geology* **40**,  
346 163–166 (2012).

347 6 Ivarsson, M., Bengtson, S., Skogby, H., Belivanova, V. & Marone, F. Fungal  
348 colonies in open fractures of subseafloor basalt. *Geo-Mar. Lett.* **33**, 233–243 (2013).

349 7 Ivarsson, M. *et al.* Zygomycetes in vesicular basanites from Vesteris Seamount,  
350 Greenland Basin – a new type of cryptoendolithic fungi. *PLoS ONE* **10**, 16 pp.,  
351 doi:10.1371/journal.pone.0133368 (2015).

352 8 Furnes, H. *et al.* in *Modern Approaches in Solid Earth Sciences* Vol. 4 (eds  
353 Yildirim Dilek, Harald Furnes, & Karlis Muehlenbachs) 1–68 (Springer, 2008).

354 9 Grosch, E. G. & McLoughlin, N. Reassessing the biogenicity of Earth’s oldest  
355 trace fossil with implications for biosignatures in the search for early life. *Proc. Natl.*  
356 *Acad. Sci. USA* **111**, 8380–8385 (2014).

357 10 Staudigel, H., Furnes, H. & DeWit, M. Paleoarchean trace fossils in altered  
358 volcanic glass. *Proc. Natl. Acad. Sci. USA* **112**, 6892–6897 (2015).

- 359 11 Grosch, E. G. & McLoughlin, N. Questioning the biogenicity of titanite mineral  
360 trace fossils in Archean pillow lavas. *Proc. Natl. Acad. Sci. USA* **112**, E1390–E1391  
361 (2015).
- 362 12 McLoughlin, N. & Grosch, E. G. A hierarchical system for evaluating the  
363 biogenicity of metavolcanic- and ultramafic-hosted microalteration textures in the  
364 search for extraterrestrial life. *Astrobiology* **15**, 901–921 (2015).
- 365 13 Fisk, M. & McLoughlin, N. Atlas of alteration textures in volcanic glass from  
366 the ocean basins. *Geosphere* **39**, 317–341 (2013).
- 367 14 Phillips, W. J. Interpretation of crystalline spheroidal structures in igneous rocks.  
368 *Lithos* **6**, 235–244 (1973).
- 369 15 McLoughlin, N., Staudigel, H., Furnes, H., Eickmann, B. & Ivarsson, M.  
370 Mechanisms of microtunneling in rock substrates: distinguishing endolithic  
371 biosignatures from abiotic microtunnels. *Geobiology* **8**, 245–255 (2010).
- 372 16 Lepot, K., Benzerara, K. & Philippot, P. Biogenic versus metamorphic origins of  
373 diverse microtubes in 2.7 Gyr old volcanic ashes: Multi-scale investigations. *Earth*  
374 *Planet Sci Lett* **312**, 37–47 (2011).
- 375 17 Pasteris, J. D. & Wopenka, B. Necessary, but not sufficient: Raman  
376 identification of disordered carbon as a signature of ancient life. *Astrobiology* **3**, 727–  
377 738 (2003).

- 378 18 Sumner, D. Y. Poor preservation potential of organics in Meridiani Planum  
379 hematite-bearing sedimentary rocks. *Journal of Geophysical Research* **109**, 8 pp.,  
380 doi:10.1029/2004JE002321 (2004).
- 381 19 Chi Fru, E. *et al.* Fossilized iron bacteria reveal pathway to biological origin of  
382 banded iron formation. *Nature Communications* **4**, 7 pp. (2013).
- 383 20 Staudigel, H., Hart, S. R. & Richardson, S. H. Alteration of the oceanic crust:  
384 processes and timing. *Earth Planet Sci Lett* **52**, 311–327 (1981).
- 385 21 Erikson, D. The morphology, cytology, and taxonomy of the Actinomycetes.  
386 *Annu. Rev. Microbiol.* **3**, 23–54 (1949).
- 387 22 Higgins, M. L. & Silvey, J. K. G. Slide culture observations of two freshwater  
388 Actinomycetes. *Trans Am Microsc Soc* **85**, 390–398 (1966).
- 389 23 Goodfellow, M. *et al.* (eds.). *Bergey's Manual of Systematic Bacteriology. 5. The*  
390 *Actinobacteria*. 2nd edn, 2083 pp. (Springer, 2012).
- 391 24 Bull, A. T. in *Extremophiles Handbook* (eds K. Horikoshi *et al.*) 1203–1240  
392 (Springer, 2011).
- 393 25 Edgcomb, V. P., Beaudoin, D., Gast, R., Biddle, J. F. & Teske, A. Marine  
394 subsurface eukaryotes: the fungal majority. *Environ. Microbiol.* **13**, 172–183 (2011).
- 395 26 Orsi, W., Biddle, J. F. & Edgcomb, V. Deep sequencing of subseafloor  
396 eukaryotic rRNA reveals active fungi across marine subsurface provinces. *PLoS ONE* **8**,  
397 1–10 (2013).

- 398 27 Sohlberg, E. *et al.* Revealing the unexplored fungal communities in deep  
399 groundwater of crystalline bedrock fracture zones in Olkiluoto, Finland. *Frontiers in*  
400 *Microbiology* **6**, 11 pp., doi:10.3389/fmicb.2015.00573 (2015).
- 401 28 Ivarsson, M., Bengtson, S. & Neubeck, A. The igneous oceanic crust – Earth’s  
402 largest fungal habitat? *Fungal Ecology* **20**, 249–255 (2016).
- 403 29 Pachiadaki, M. G., Rédou, V., Beaudoin, D. J., Burgaud, G. & Edgcomb, V. P.  
404 Fungal and prokaryotic activities in the marine subsurface biosphere at Peru margin and  
405 Canterbury Basin inferred from RNA-based analyses and microscopy. *Frontiers in*  
406 *Microbiology* **7**, 16 pp., doi:10.3389/fmicb.2016.00846 (2016).
- 407 30 Nicolson, T. H. Mycorrhiza in the gramineae. 1. Vesicular-arbuscular  
408 endophytes, with special reference to the external phase. *Journal of the British*  
409 *Mycological Society* **42**, 421–438 (1959).
- 410 31 Glass, N. L., Rasmussen, C., Roca, M. G. & Read, N. D. Hyphal homing, fusion  
411 and mycelial interconnectedness. *Trends Microbiol.* **12**, 135–141 (2004).
- 412 32 Bengtson, S. *et al.* Deep-biosphere consortium of fungi and prokaryotes in  
413 Eocene sub-seafloor basalts. *Geobiology* **12**, 489–496 (2014).
- 414 33 Ivarsson, M. *et al.* A fungal-prokaryotic consortium at the basalt-zeolite  
415 interface in subseafloor igneous crust. *PLoS ONE* **10**, 19 pp.,  
416 doi:10.1371/journal.pone.0140106 (2015).

417 34 Brown, J. W. & Sorhannus, U. Autotrophic stramenopiles (Ochrophyta):  
 418 substantive underestimation of putative fossil ages. *PLoS ONE* **5**, 11 pp.,  
 419 doi:10.1371/journal.pone.0012759 (2010).

420 35 Stephenson, L. W., Erwin, D. C. & Leary, J. V. Hyphal anastomosis in  
 421 *Phytophthora capsici*. *Phytopathology* **64**, 149–150 (1974).

422 36 Sbrana, C., Nuti, M. P. & Giovannetti, M. Self-anastomosing ability and  
 423 vegetative incompatibility of *Tuber borchii* isolates. *Mycorrhiza* **17**, 667–675 (2007).

424 37 Dowson, C. G., Boddy, L. & Rayner, A. D. M. Development and extension of  
 425 mycelial cords in soil at different temperatures and moisture contents. *Mycol. Res.* **92**,  
 426 383–391 (1989).

427 38 Cavalier-Smith, T. & Chao, E. E. The opalozoan *Apusomonas* is related to the  
 428 common ancestor of animals, fungi, and choanoflagellates. *Proceedings of the Royal*  
 429 *Society of London. B. Biological Sciences* **261**, 1–6 (1995).

430 39 James, T. Y. *et al.* Reconstructing the early evolution of Fungi using a six-gene  
 431 phylogeny. *Nature* **443**, 818–822 (2006).

432 40 Baldauf, S. L. An overview of the phylogeny and diversity of eukaryotes.  
 433 *Journal of Systematics and Evolution* **46**, 263–273 (2008).

434 41 Heckman, D. S. *et al.* Molecular evidence for the early colonization of land by  
 435 fungi and plants. *Science* **293**, 1129–1133 (2001).

436 42 Hedges, S. B., Blair, J. E., Venturi, M. & Shoe, J. L. A molecular timescale of  
437 eukaryote evolution and the rise of complex multicellular life. *BMC Evol. Biol.* **4**, 1–9  
438 (2004).

439 43 Padovan, A. C. B., Sanson, G. F. O., Brunstein, A. & Briones, M. R. S. Fungi  
440 evolution revisited: application of the penalized likelihood method to a Bayesian fungal  
441 phylogeny provides a new perspective on phylogenetic relationships and divergence  
442 dates of Ascomycota groups. *J. Mol. Evol.* **60**, 726–735 (2005).

443 44 Bhattacharya, D., Yoon, H. S., Hedges, S. B. & Hackett, J. D. in *The Timetree of*  
444 *Life* (eds S.B. Hedges & S. Kumar) 116–120 (Oxford UP, 2009).

445 45 Parfrey, L. W., Lahr, D. J. G., Knoll, A. H. & Katz, L. A. Estimating the timing  
446 of early eukaryotic diversification with multigene molecular clocks. *Proc. Natl. Acad.*  
447 *Sci. USA* **108**, 13624–13629 (2011).

448 46 Taylor, T. N., Krings, M. & Taylor, E. L. *Fossil Fungi*. 382 pp. (Elsevier,  
449 2015).

450 47 Sharpe, S. C., Eme, L., Brown, M. W. & Roger, A. J. in *Evolutionary*  
451 *Transitions to Multicellular Life* (eds Iñaki Ruiz-Trillo & Aurora M. Nedelcu) 3–29  
452 (Springer, 2015).

453 48 Kohlmeyer, J. & Kohlmeyer, E. *Marine Mycology*. (Academic Press, 1979).

454 49 Benton, M. J. *et al.* Constraints on the timescale of animal evolutionary history.  
455 *Palaeontol Electron* **18**, 107 pp. (2015).

456 50 Johnson, J. E., Gerpheide, A., Lamb, M. P. & Fischer, W. W. O<sub>2</sub> constraints  
457 from Paleoproterozoic detrital pyrite and uraninite. *GSA Bulletin* **126**, 813–830 (2014).

458 51 Lanari, P. *et al.* XMapTools: A MATLAB©-based program for electron  
459 microprobe X-ray image processing and geothermobarometry. *Comput Geosci* **62**, 227–  
460 240 (2014).

461 52 Bourdelle, F., Parra, T., Chopin, C. & Beyssac, O. A new chlorite  
462 geothermometer for diagenetic to low-grade metamorphic conditions. *Contributions to*  
463 *Mineralogy and Petrology* **165**, 723–735 (2013).

464 53 Marone, F. & Stampanoni, M. Regridding reconstruction algorithm for real-time  
465 tomographic imaging. *Journal of Synchrotron Radiation* **19**, 1029–1037 (2012).

466 **Acknowledgements** Our work has been supported by the Agouron Institute, Swedish  
467 Research Council (2012-4364, 2013-4290), Danish National Research Foundation  
468 (DNRF53), Australian Research Council (DP110103660, DP140100512), Paul Scherrer  
469 Institute (20130185, 20141047), Australian Microscopy & Microanalysis Research  
470 Facility, National Science Foundation (EAR-05-45484), NASA Astrobiology Institute  
471 (NNA04CC09A), Natural Sciences and Engineering Research Council, and the  
472 European Commission CALIPSO programme (312284). We thank V. Belivanova for  
473 technical assistance, P. von Knorring for drafting Supplementary Fig. 6, J. Peckmann  
474 for supplying images for Supplementary Fig. 8c, d, and A. Tehler for discussions.

475 **Author Contributions** A.B. provided the material and geological information; B.R.  
476 discovered the filamentous structures; S.B., B.R., and M.I. designed the study; S.B.,  
477 B.R., M.I., J.M., and C.B. performed the investigation; S.B. and B.R. wrote the paper

478 with input from other co-authors; M.S. and F.M. designed and operated the TOMCAT  
479 beamline.

480 **Author Information** The authors declare no competing financial interests.

481 Correspondence should be directed to S.B. (stefan.bengtson@nrm.se) or B.R.

482 (b.rasmussen@curtin.edu.au).

## 483 Figure captions

484 **Figure 1 | Geological map and stratigraphic section of the Griqualand West sub-**  
485 **basin**, showing the location of Agouron drillhole GTF01 (S28°49'39.7"  
486 E023°07'24.1"). The fossiliferous sample is from the lower part of the Ongeluk  
487 Formation (drill depth 21.79 m). Modified after Ref.<sup>50</sup>.

488 **Figure 2 | Ongeluk vesicular basalt with filamentous fossils, petrographic thin**  
489 **sections. a–i**, Transmitted light; **j–l**, ESEM images, backscatter mode. **a**, Basalt with  
490 vesicles frequently connected by veins; Swedish Museum of Natural History X6129. **b**,  
491 **c**, Anastomosing network; X6130. **d**, **e**, Vesicle with broom structure; note distinction  
492 between calcite (light) and chlorite (dark) cement; X6131. **f**, Anastomosis; X6132. **g**,  
493 Broom structure in fracture (same specimen as in Fig. 4); X6133. **h**, Broom; X6134. **i**,  
494 Vesicle connected to vein filled with calcite (light) and chlorite (dark) cement; X6135.  
495 **j–l**, Basal film and marginal network; X6136. Legend: an, anastomosis; bf, basal film;  
496 Ca, calcite; Chl1, Chlorite 1; hy, hypha; ve, vein; Yj, Y-junction.

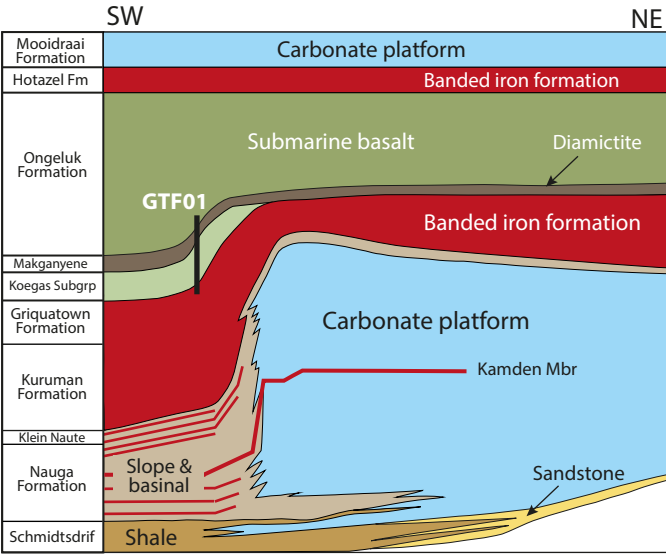
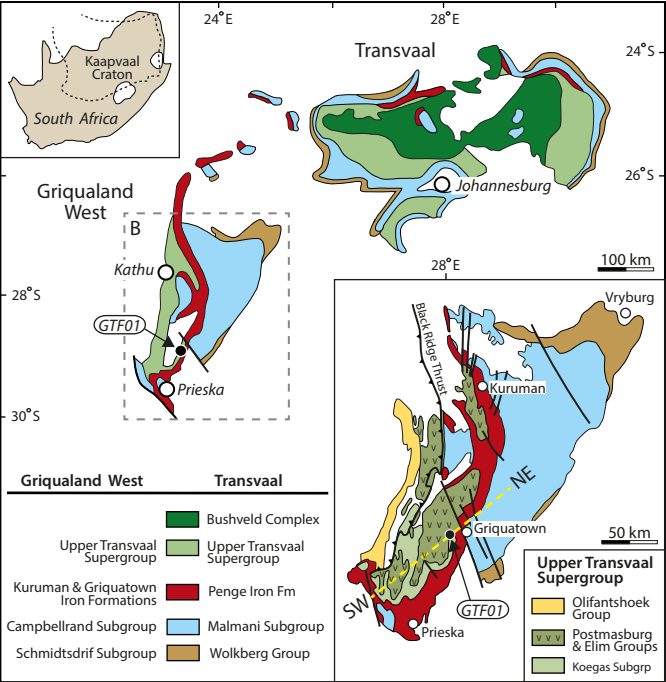
497 **Figure 3 | Ongeluk vesicle with filamentous fossils, SRXTM surface/volume**  
498 **renderings**; Swedish Museum of Natural History X6137. Legend: an, anastomosis; bf,

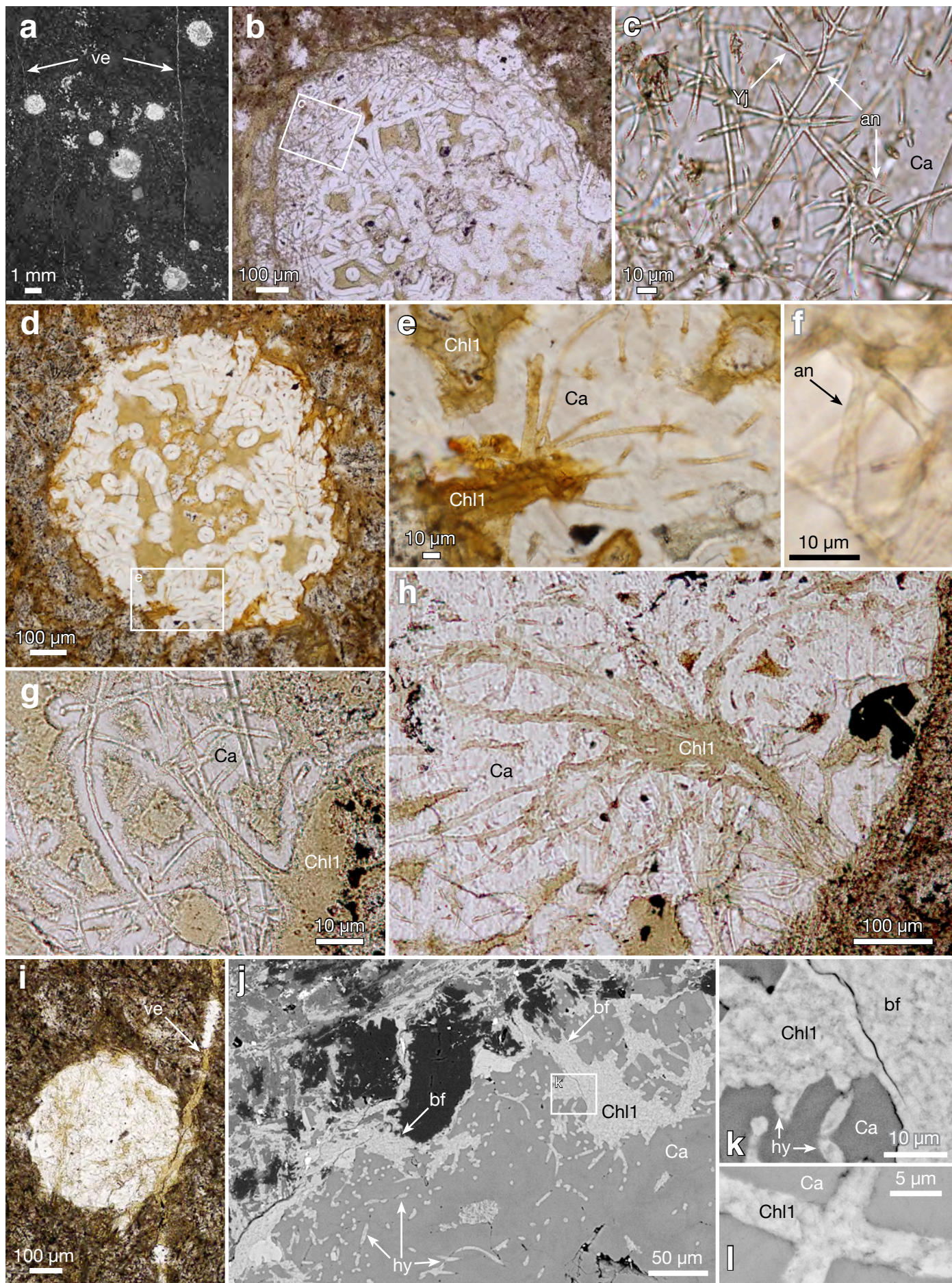
499 basal film; bp, bulbous protrusion; br, broom; fb, false branching; lo, loop; tf, touching  
500 filaments; Tj, T-junction; Yj, Y-junction.

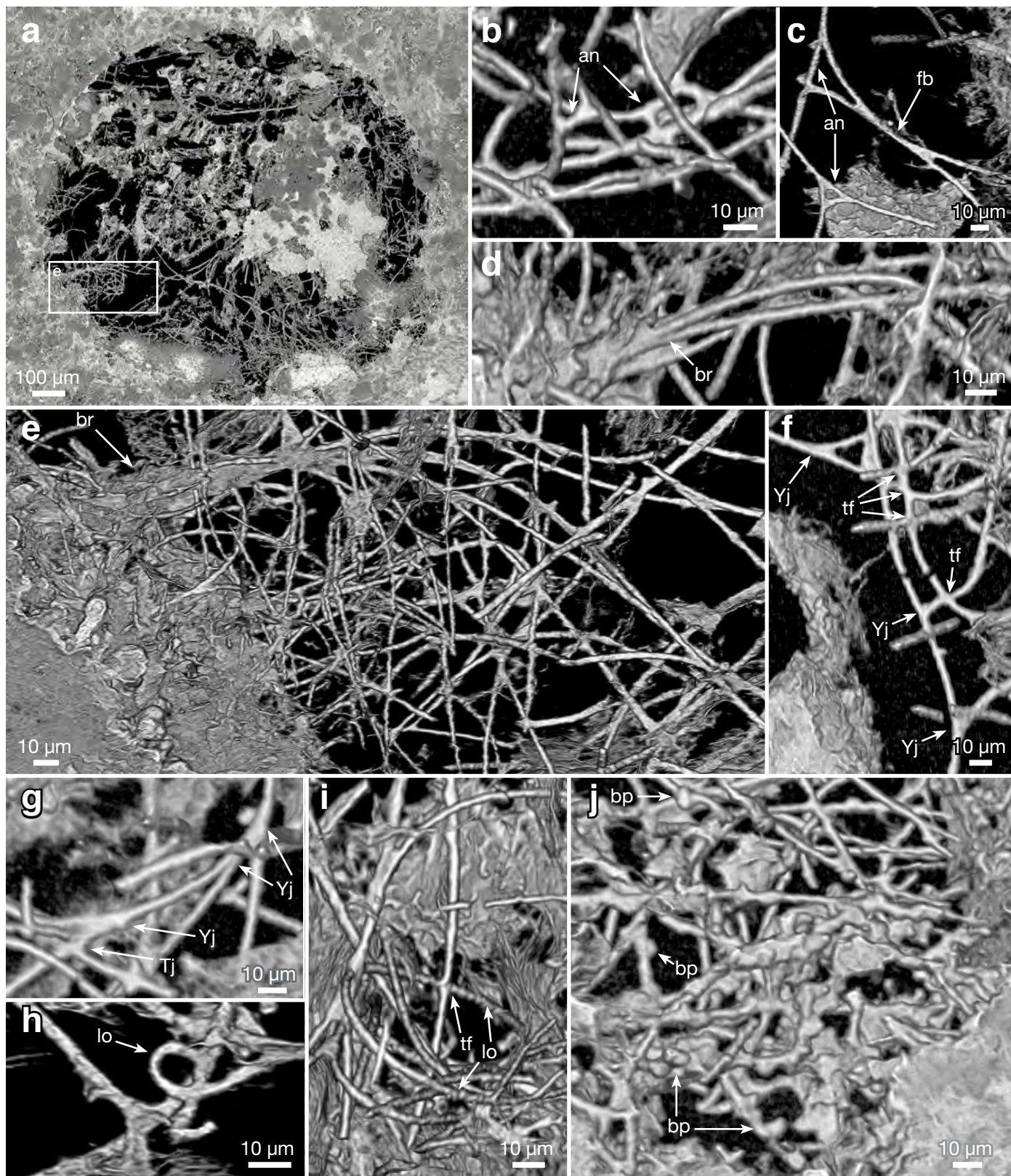
501 **Figure 4 | Calcite- and chlorite-filled fracture with filamentous fossils in Ongeluk**  
502 **vesicular basalt, petrographic thin section;** Swedish Museum of Natural History  
503 X6133. a–d, Plane-polarized transmitted light; e, Crossed nicols. Fracture truncated  
504 along centre by edge of section (a, top). Fracture filling divided into central zone and  
505 peripheral filamentous zone, parted by a band of Chlorite 2; note truncation of filaments  
506 by Chlorite 2 band (c–e). Different intensity of calcite interference colours in  
507 filamentous zone (e) indicates blocky distribution of calcite crystals, not related to  
508 filament morphology; chloritic filaments are too thin to reveal interference colours of  
509 Chlorite 1 (black arrow). Legend: Ca, calcite; Chl1, Chlorite 1; Chl2, Chlorite 2.

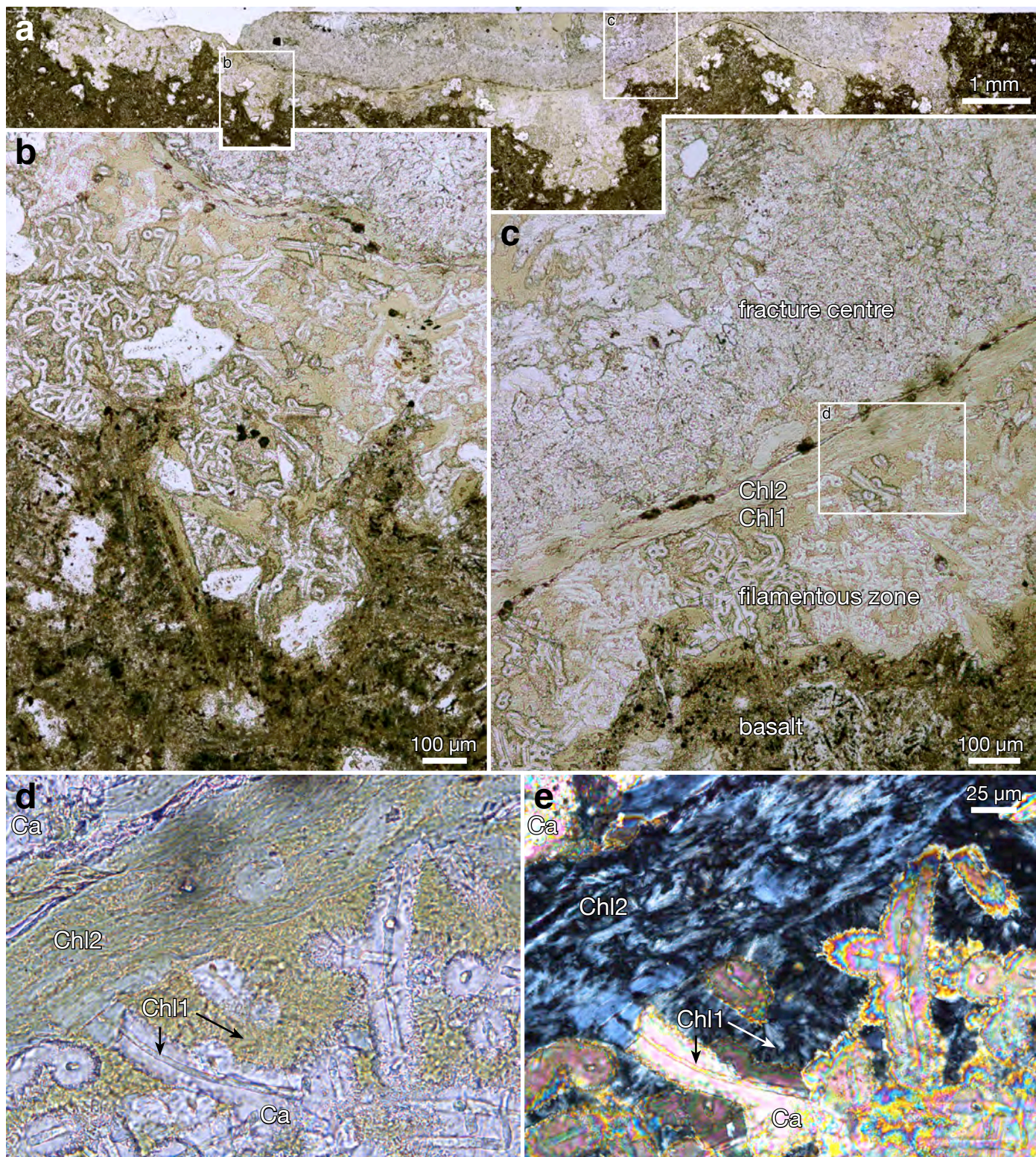
510

511









# Fungus-like mycelial fossils in 2.4 billion-year-old vesicular basalt

Stefan Bengtson, Birger Rasmussen, Magnus Ivarsson, Janet Muhling, Curt Broman, Federica Marone, Marco Stampanoni and Andrey Bekker

## Supplementary Information

### Geological setting

The Ongeluk Formation is up to 900 m thick and comprises mainly massive basalt, hyaloclastites and pillow lavas that extruded under seawater<sup>1,2</sup>. Individual flows are typically 2–3 m thick and contain amygdales towards the top. Flows may be capped by flow breccias and separated from overlying flows by thin layers of sediment and jasper<sup>2</sup>. The lavas have undergone a remarkably low degree of deformation and only very low-grade (sub-greenschist) metamorphism<sup>3</sup>. Geochemical and petrographic data indicate that the basalts have undergone low-temperature alteration by seawater after extrusion<sup>2</sup>.

The basalts are grey to green and preserve igneous textures ranging from subophitic and intergranular to intersertal and glomeroporphyritic<sup>4</sup>. They contain mainly augite and plagioclase laths with minor ilmenite, zircon and titanomagnetite. The primary minerals have undergone alteration, with the growth of chlorite, pumpellyite, quartz, albite, calcite and sulphide minerals. Vesicles and fractures are commonly filled with chlorite, calcite, quartz and sulphides.

An earlier generated Pb–Pb isochron has indicated a ca. 2.2 Ga eruption age of the basalt<sup>2</sup>. However, whole-rock U–Pb and Pb–Pb isochron ages from dolomite of the overlying Mooidraai Formation suggest that the Ongeluk Formation is older than 2.39 Ga<sup>5,6</sup>, and U–Pb dating of baddeleyite in sub-volcanic sills in the lower part of the Ongeluk Formation gives an age of ca. 2426±3 Ma<sup>7</sup>.

The timing of metamorphism of the Ongeluk Formation is uncertain, but significant seafloor alteration apparently occurred shortly after extrusion<sup>2</sup>. The mineral assemblages of the basalts may also have been affected by later episodes of metamorphism, although direct dates for these are lacking. In situ U–Pb geochronology of monazite, xenotime and titanite in the Transvaal Supergroup sediments indicates that the Kaapvaal craton has been affected by regional events at ~2.15 Ga and ~2.06 Ga<sup>8,9</sup>. Paleomagnetic data from the Kalahari mineral field suggests a complex thermal history with possible events at ~1.9 Ga, 1.8–1.75 Ga and

1.25–1.1 Ga<sup>10</sup>. A paleosol developed on the Ongeluk Formation yielded a Rb/Sr date of 1257±11 Ma<sup>11</sup>, which may represent localized metasomatic alteration along faults and lithological contacts.

### Vesicles vs. varioles

A number of different spherical or globular structures are found in volcanic and subvolcanic rocks (see Phillips, 1973<sup>12</sup>, for nomenclature and brief descriptions). The most common are vesicles, formed due to the exsolution of a vapour phase and formation of gas bubbles from the magma as it rises to the Earth's surface. Vesicles are found in all types of magma, in subaerial and submarine volcanic rocks, in pillowed and non-pillowed basaltic rocks. They form cavities, called amygdales (or amygdules), in many cases filled by secondary, low-temperature, minerals. The minerals forming the amygdales nucleate on the walls of the vesicles and grow inwards to fill the empty space. The most common minerals forming amygdales are zeolites, clays, chlorite, chalcedony, quartz, barite and calcite. In Precambrian rocks, which have experienced at least low-temperature metamorphism, zeolites and clay minerals are generally replaced by chlorite, other phyllosilicates and in some cases, low-temperature feldspars, while quartz and calcite are recrystallized.

Varioles are centimeter-scale, leucocratic spherical or globular structures found in basaltic rocks. They are comparatively common in, although not restricted to, Archaean basalts. They are mostly composed of feldspars that show radial growth from the centre of the variole outwards. They generally result from spherulitic growth of plagioclase, which may be nucleated on an amygdale or crystal nucleus<sup>13,14</sup>. They grow from a point outwards, in contrast to amygdales. The feldspars within variolitic spherulites may have a dendritic habit. Dendrites are characterized by branching from a central 'stem' and are crystallographically controlled. The stem and branches become progressively finer away from the point of origin, and there is a regular arrangement of side branches. Less commonly, varioles result

from the crystallization of droplets of felsic magma in mafic magma, due to mixing of magmas with different composition. These varioles have the compositions of magmas.

The spherical structures that we describe from the Ongeluk lavas do not have the composition of magmas and do not have a spherulitic, i.e. radial, structure. They are <2 mm in diameter and filled with minerals, e.g., calcite, quartz and chlorite, that are characteristic of amygdalites. Amygdalites containing these minerals are common in the Ongeluk lavas<sup>2</sup>, whereas varioles have not been described from there.

## Chlorite thermometry

Chlorite defining the filament structures was analysed from two amygdalites containing microfossil filaments in Thin Section IOS004 (Supplementary Table 1). The chlorite comprises aggregates of very fine grains (<1 µm), so analyses are derived from composites rather than single grains. Minor amounts of CaO are recorded in all analyses, suggesting that the aggregates include some fine calcite as well as chlorite. Analyses with >1 wt% CaO have been excluded from the temperature calculations. The chlorites are Fe-rich members of the chamosite–clinocllore series (Mg numbers 0.35–0.37) with ~0.9 apfu (atoms per formula unit based on 14 oxygen atoms) of tetrahedral Al and 1.1 apfu octahedral Al (Supplementary Table 1). Temperatures were estimated following the method of Bourdelle et al.<sup>15</sup>, which is independent of the oxidation state of Fe and applicable to chlorites formed at temperatures <300°C. Temperature estimates for chlorite in the two amygdalites are indistinguishable, and seven analyses give temperatures in the range 198–234°C with an average of 209±14°C (2σ).

Chlorites from both amygdalites and groundmass were analysed in Thin Section ZBF061 (Supplementary Table 2). The amygdalites contain very fine-grained chamosite (Chlorite 1) associated with poorly defined microfossil filaments as in Section IOS004, but also some pale-green, coarser-grained flakes (Chlorite 2). In some places, Chlorite 2 forms overgrowths on Chlorite 1. The Chlorite 1 is chamosite with only minor Ca in some analyses and has Mg numbers of 0.31–0.36 and ~0.8–0.9 apfu tetrahedral Al and 1.0–1.3 apfu octahedral Al, similar to Section IOS004. Temperature estimates from the Bourdelle thermometer range from 179°C to 260°C with an average of 202±26°C (n=16) from EDS analyses and 211±29°C (n=25) from WDS analyses.

Chlorite 2 is more Fe-rich and aluminous, with no Ca, and Mg numbers 0.24–0.26. It has 1.2–1.3 apfu tetrahedral Al and 1.3–1.4 apfu octahedral Al. Temperatures estimated using the Bourdelle et al. calibration<sup>15</sup> are >300°C and therefore out of the range employed in the calibration of this thermometer. The thermometer of Lanari et al.<sup>16</sup> is applicable for chlorites with <3 apfu Si and a crystallization temperature up to 500°C. The formulation where all Fe is treated as Fe<sup>2+</sup> and vacancies are >0.03 (thermometer 2 of Lanari et al.<sup>16</sup>) is appropriate for the analyses of Chlorite 2 and gives temperatures in the range 319–411°C with an average of 368±33°C (n=10) for EDS analyses and 335±67°C (n=22) for WDS analyses.

The groundmass of the basalt in thin section ZBF061 has been totally altered, with plagioclase laths replaced by K-feldspar and more mafic minerals and interstitial groundmass or glass by fine-grained chlorite, quartz, K-feldspar and calcite. The age relationship between the chlorite in the groundmass and chlorite in the amygdalites is not clearly defined. The composition of the chlorite in the groundmass is intermediate between Chlorite 1 and Chlorite 2. It has Mg numbers 0.25–0.29, and 1.2–1.4 apfu octahedral Al and 1.0–1.2 apfu tetrahedral Al. Both the Bourdelle and Lanari thermometers are applicable to these analyses. Temperature estimates for seven analyses have a range of 214–304°C with an average of 262±34°C (thermometer of Bourdelle et al.<sup>15</sup>) and 121–278°C with an average of 232±54°C (thermometer of Lanari et al.<sup>16</sup>). These estimates overlap within the accuracy of the methods, which is estimated at ±30°C.

## Raman carbonaceous-material geothermometry

The ordering of the structure of carbonaceous material (CM) reflects the maximum metamorphic temperature condition that has affected the carbon compound in the rock, and the transformation of the structure from its original carbonaceous precursor is irreversible during retrogression. The temperature–CM structure relationship can therefore be used as a geothermometer<sup>17,18</sup>. In order to characterize the CM, Raman spectrometry was performed on thin sections of the volcanic matrix in the lower part of the Ongeluk Formation, a basal sandstone in the Ongeluk Formation, and from a diamictite of the underlying Makganyene Formation. Inspections for the presence of CM were also made of a dolerite dyke immediately above the Ongeluk sample and of calcite-filled cavities from the lower part of the Ongeluk Formation. All spectra were recorded on CM below the sample surface and with low laser power to avoid laser-induced modifications of the CM. The Raman spectra of CM<sup>17,18</sup> have a first-order region with two main bands at ~1350 (D1) and ~1580 cm<sup>-1</sup> (G) together with minor bands at ~1250 cm<sup>-1</sup> (D4) as a shoulder on D1, a wide band at ~1510 cm<sup>-1</sup> (D3) and at ~1620 cm<sup>-1</sup> (D2) as a shoulder on G. Second-order overtone bands occur in the region 2600–3200 cm<sup>-1</sup>. The G band is the only band in well-ordered graphite and with increasing disorder structure, the D1, D2, D3 and D4 bands appear. The D1 band becomes more wide and intense with decreasing order of the CM, and the width of D2, D3 and D4 increases. In poorly ordered CM it is impossible to separate the G and D2 bands, and thus only one broad band is observed at ~1600 cm<sup>-1</sup>. The obtained Raman spectra are shown in Supplementary Fig. 7 where the difference of the CM structures between the Ongeluk and the Makganyene samples is clearly demonstrated. There was no CM detected neither in the dolerite (Supplementary Fig. 7) nor in the calcite-filled cavities including the hyphae fossils (Supplementary Fig. 2). For the Raman CM geothermometer at temperatures above 330°C, Beyssac et al.<sup>17</sup> proposed that there is a linear correlation of the band area ratio  $R2 = D1 / (D1 + G + D2)$  and the

temperature  $T$  ( $^{\circ}\text{C}$ ), according to the equation  $T = -445 \times R2 + 641$ . The ratios of the band areas measured on 10 isolated CM from the Makganyene diamictite and the Ongeluk sandstone are between 0.59 and 0.61 suggesting an average maximum temperature of around  $370^{\circ}\text{C}$ . The shape of the Raman spectra for the CM in the matrix of the Ongeluk volcanic sample (Supplementary Fig. 7b) with a wide D1 band, visible D4 shoulder, a wide G and D4 that cannot be separated, high intensity of the D3 band and significantly suppressed second-order bands points to a poorly ordered structure and low ( $<300^{\circ}\text{C}$ ) metamorphic temperature<sup>17,18</sup>. For temperatures below  $300^{\circ}\text{C}$ , the band height ratio  $R1 = D1/G$  changes regularly with metamorphic grade, and based on this Rahl et al.<sup>18</sup> presented a modified Raman CM geothermometer using the equation  $T = 737.3 + 320.9(R1) - 1067(R2) - 80.638(R1)^2$ . The  $R1$  ratios of five spot measurements on the Ongeluk CM range from 0.65 to 0.75 and  $R2$  values around 0.65–0.70. To determine the  $R1$  and  $R2$  values, the spectra were decomposed into D1/G bands with Lorentzian shape using the LabSpec 5 software. With this method an approximate temperature of  $200 \pm 30^{\circ}\text{C}$  was obtained. However, the shape of the bands together with the rare occurrence of CM in the Ongeluk volcanic sample gives a high uncertainty in estimates of temperatures from the spectra.

## Assessment of antiquity and biogenicity

In the following we investigate how the Ongeluk filaments stand up against criteria of antiquity and biogenicity established in the recent literature<sup>19,20</sup> for ancient microfossil-like structures. We have chosen this approach, rather than setting up our own list of criteria, in order to avoid the possibility of ad-hoc rules potentially adding bias to the comparisons. Lines in boldface denote the fulfillment (or non-fulfillment) of the criteria by the Ongeluk structures.

The following list of criteria distinguishing crypto- and chasmoendolithic filaments from biogenic and abiogenic tunnels in rock was set up by McLoughlin et al.<sup>19</sup>.

### *Cryptoendolithic filaments*

Timing of formation: Pre-metamorphic growth into a fluid-filled cavity.

**Criterion fulfilled.**

Morphology: Filaments with circular cross-section, of a non-uniform diameter are curvilinear, or branched, and may show swellings along their lengths.

**Criterion fulfilled.**

Infilling mineralogy: Clays with or without organics.

**Criterion fulfilled.**

Host matrix: Carbonate-filled vesicles.

**Criterion fulfilled.**

Distribution: Grow into cavities.

**Criterion fulfilled.**

Mechanical abrasion: No.

**Criterion fulfilled.**

Dissolution: Possibility of secondary chemical dissolution.

**Criterion fulfilled.**

### *Chasmoendolithic filaments*

Timing of formation: Pre-metamorphic growth into a fluid-filled vein or fracture.

**Criterion fulfilled.**

Morphology: Filaments with circular cross-section, of non-uniform diameter, may be curvilinear, branched, show internal septae or terminal swellings.

**Criterion fulfilled.**

Infilling mineralogy: Iron-oxides or clays.

**Criterion fulfilled.**

Host matrix: Carbonate or zeolite-filled veins.

**Criterion fulfilled.**

Distribution: Grow into fluid-filled vein or fracture, nucleate on walls.

**Criterion fulfilled.**

Mechanical abrasion: No.

**Criterion fulfilled.**

Dissolution: Possibility of secondary chemical dissolution.

**Criterion fulfilled.**

The following list of antiquity and biogenicity criteria for ancient microfossils is adopted from Wacey<sup>20</sup>.

### *General antiquity criteria*

(1) Structures must occur in rocks of known provenance; i.e., detailed location information must be presented so that independent re-sampling is possible.

**Criterion fulfilled; sample is from specified drill core.**

(2) Structures must occur in rocks of demonstrable or established age; i.e., the host rock must be dated directly by radiometric techniques, or the age of the rocks can be accurately inferred by correlation to nearby rocks that have been dated.

**Criterion fulfilled; see “Supplementary Information: Geological Setting”.**

(3) Structures must be indigenous to the primary fabric of the host rock; i.e., they must be physically embedded within the rock, not products of sample collection or preparation. They should, therefore, be present in petrographic thin sec-

tions of the rock. Other identification techniques such as acid maceration and acid etching are valuable accessory techniques but may accidentally incorporate post-depositional contaminants.

**Criterion fulfilled; specimens are identified in petrographic sections as well as in closed vesicles examined by X-ray techniques.**

(4) Structures must be syngenetic with the primary fabric of the host rock; i.e., they must not have been introduced by ancient or modern post-depositional fluids.

**Criterion not relevant to cryptoendolithic biota, which by definition occupies cavities in already existing rock.**

(5) Following from 4; any structures found within metastable mineral phases, void filling cements, veins, or cross-cutting fabrics must be viewed with extreme caution.

**See comments to point 4 above.**

(6) Structures should not occur in high-grade metamorphic rocks, because delicate organic structures will not survive these extremes of pressure and/or temperature; the likelihood of non-biological artefacts in such rocks is substantially increased.

**Criterion fulfilled; chlorite thermometry shows that the low-grade metamorphism represented by Chlorite 2 has not affected crystals of Chlorite 1 replicating the fossil filaments.**

(7) The geological context of the host rock must be fully understood at a range of scales; i.e., the host unit must show geographical extent and fit logically within the regional geological history.

**Criterion fulfilled; see “Supplementary Information: Geological setting”.**

### ***Additional antiquity criteria specific to microfossils***

(8) Potential microfossils should not be significantly different in colour from that of particulate carbonaceous material in the remainder of the rock matrix. For example, brown ‘microfossils’ in a largely black carbonaceous chert would immediately be suspicious.

**Criterion not applicable to non-organic preservation, as in the Ongeluk structures.**

(9) There should be evidence for organo-sedimentary interaction, e.g., sediment grains trapped or supported by fossils, coatings of distinctive composition or texture precipitated around the fossils, or perhaps alternating layers of prostrate and erect filaments in stromatolite-like sediments.

**Criterion not applicable to non-sedimentary environments.**

### ***General biogenicity criteria***

(10) Structures should exhibit biological morphology that can be related to extant cells, sheaths, traces of activity or waste products. Ideally life cycle variants should be identifiable (reproductive stages), comparable to that found in morphologically similar modern or fossil microorganisms.

**Criterion fulfilled; filaments closely comparable to hyphae of Phanerozoic and modern fungi.**

(11) More than a single step of biology-like processing should be evident. These steps may take the form of biominerals (e.g., pyrite), geochemical fractionations of isotopes (e.g., carbon and sulphur), specific organic compounds (e.g., hopanoid biomarkers) or distinctive elemental ratios.

**Criterion not fulfilled; neither the calcite nor the chlorites in the amygdalae appear to be biological in origin, and there are no preserved organics.**

(12) Structures should occur within a geological context that is plausible for life; i.e., at temperatures and pressures that extant organisms are known to survive.

**Criterion fulfilled; vesicles in lavas are known to harbour cryptoendoliths.**

(13) Structures should fit within a plausible evolutionary context.

**Criterion fulfilled with question; current understanding of eukaryote evolution has fungi evolving considerably later.**

(14) Structures should be abundant and ideally occur in a multi-component assemblage.

**Criterion fulfilled in so far as the filaments are abundant within the basalt vesicles, but no direct evidence for the presence of other taxa has been found.**

(15) Following from 14, ideally they should show colonial/community behaviour.

**Criterion fulfilled; the filaments form mycelium-like structures.**

(16) Following from 15, a preferred orientation indicating a role in the formation of biofabrics would be an additional bonus criterion.

**Criterion fulfilled; the filaments are consistently organized within the vesicles.**

### ***Additional biogenicity criteria specific to microfossils***

(17) Microfossils should ideally be composed of kerogenous carbon. However, if mineralised this should be a result of microbially mediated precipitation. Later mineral replacement of carbonaceous material may also be permissible but then doubts upon antiquity will be raised.

**Criterion fulfilled in the “permissible” sense that filaments have been replaced by chlorite. The antiquity is-**

**sue, however, is dealt with using the known sequence of metamorphism of the rock (see below).**

(18) Microfossils should be largely hollow. Cell walls and sheaths are by far the most likely parts of the microbe to be preserved; cellular constituents are rarely preserved in more modern examples. Mineral artefacts are unlikely to be hollow.

**Criterion not fulfilled; filaments are preserved as solid chlorite without internal cavities.**

(19) Ideally the microfossils should show some sort of cellular elaboration; e.g., not just smooth cell walls.

**Criterion not applicable to fungal mycelia.**

(20) Microfossils should show taphonomic degradation; i.e., collapse of cells, folding of films, fracturing. This may not occur in exceptional preservational circumstances, for example, in situ rapid silicification of living communities.

**Criterion not fulfilled; no obvious taphonomic degradation, but fossilization processes inside basalt vesicles are poorly understood.**

(21) The object must exceed the minimum size for independently viable cells ( $\sim 0.25 \mu\text{m}$  diameter). Note: The recent discovery of nano-bacteria may modify this criterion to even smaller sizes.

**Criterion fulfilled; filaments concur in size with fungal hyphae.**

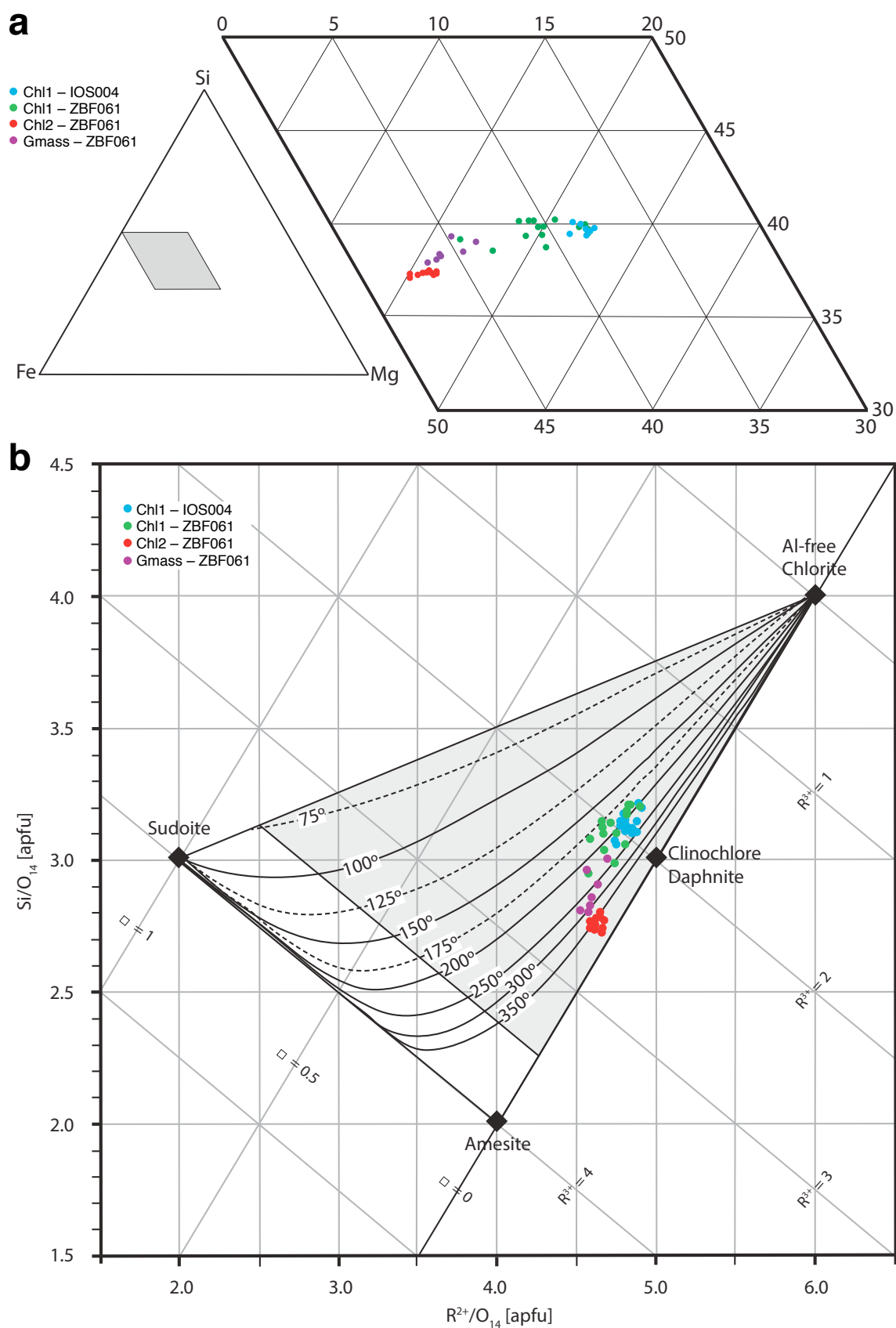
(22) Microfossils should be demonstrably dissimilar from potentially co-existing non-biological organic bodies (e.g., self organising spherulitic structures), and should occupy a restricted biological morphospace.

**Criterion fulfilled; structures well defined in shape and distinctly different from known non-biological features in similar environments.**

(23) Evidence of extra-cellular polymeric substances surrounding the putative microfossils would be an added bonus criterion.

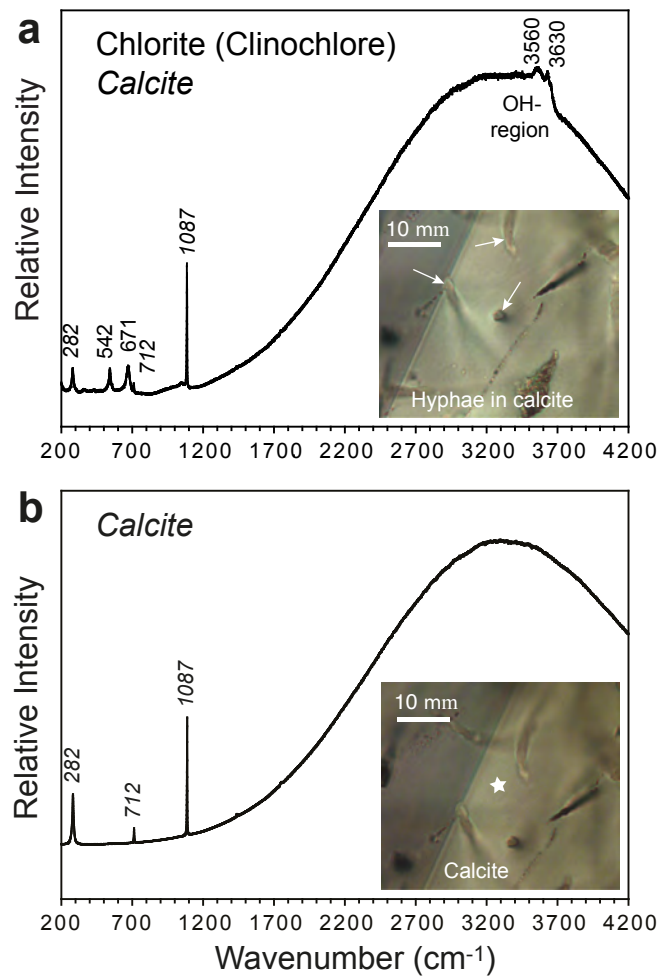
**Criterion not applicable to fungal hyphae.**

The Ongeluk filaments thus fulfill the criteria of McLoughlin et al. 2010<sup>19</sup> for crypto- and chasmoendoliths. They also meet Wacey's<sup>20</sup> relevant criteria for antiquity and biogenicity, with the exception of three (11, 18 and 20) that relate to taphonomic breakdown and hollowness of fossil structures. None of the three can be considered compelling in the case of fossils being preserved by diagenetic/metamorphic mineralization in basaltic vesicles. The fossil filaments are composed of chlorite that probably formed from smectite during metamorphism and are encased in calcite cement. This sequence of mineral growth is consistent with observations from vesicles that preserve microfossils in younger basalts<sup>21-23</sup> and with the main stages of mineral growth during the low-temperature alteration of oceanic crust<sup>24</sup>. Isotopic dating of secondary minerals in submarine basalts suggests that smectite synthesis occurs within three million years of eruption whereas calcite cementation is complete within 10 million years<sup>24</sup>, suggesting that cavities in the Ongeluk basalt were largely occluded within 10 million years of eruption. Some time after burial, likely during metamorphism at  $\sim 2.15 \text{ Ga}$  and/or  $\sim 2.06 \text{ Ga}$ <sup>8</sup>, the clays that mineralized the filaments, as well as clays within the vesicles and the matrix of the basalts, were converted to Chlorite 1 at crystallization temperatures of  $179\text{--}260^\circ\text{C}$ , followed by a partial recrystallization to Chlorite 2 at  $319\text{--}411^\circ\text{C}$  (see "Chlorite Thermometry" above).

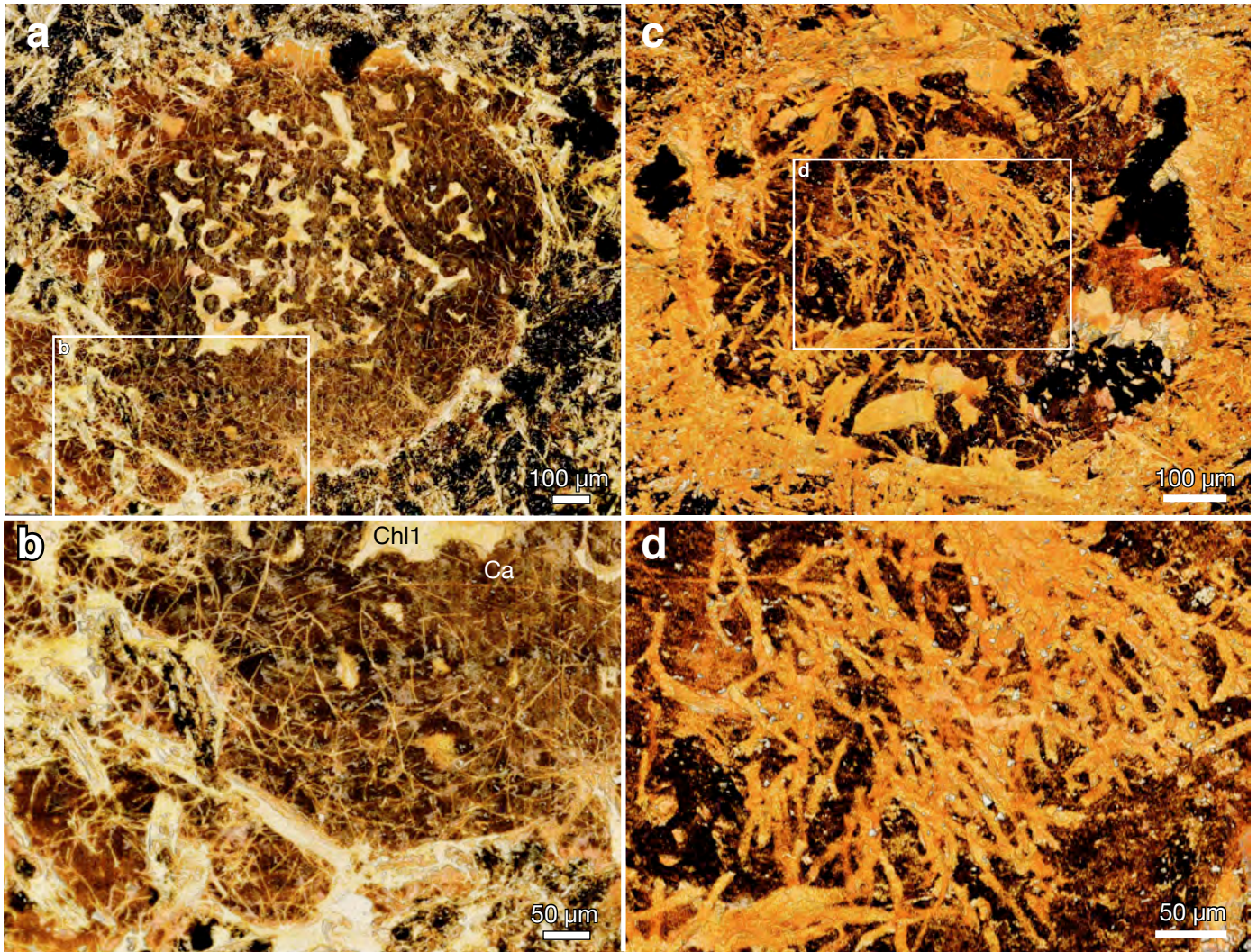


**Supplementary Figure 1 | Plots showing chlorite composition. a,** Compositions of Chlorite 1 from amygdals in IOS004 and ZBF061, Chlorite 2 from an amygdale in ZBF061, and Chlorite from the groundmass of ZBF061 in a triangular Si-Fe-Mg composition diagram. Chlorite 1 and Chlorite 2 are compositionally distinct, while groundmass chlorite falls between Chlorite 1 and Chlorite 2. **b,** Chlorite compositions plotted on the graphical chlorite thermometer of Bourdelle and Cathelineau<sup>25</sup>. R<sup>2+</sup> represents divalent cations

(Fe, Mg), R<sup>3+</sup> represents trivalent cations (Al, Fe) and  $\square$  represents vacancies in atoms per formula unit (apfu) in chlorite based on 14 oxygen atoms. The shaded area is the compositional space for which the Bourdelle et al.<sup>15</sup> thermometer is calibrated. The compositions of Chlorite 1 have >3.0 Si apfu and indicate crystallization temperatures of 175–250°C; Chlorite 2 compositions have <3.0 apfu Si and cluster around temperatures  $\geq 350^\circ\text{C}$ ; Compositions and temperatures for groundmass chlorite plot between Chlorite 1 and Chlorite 2.

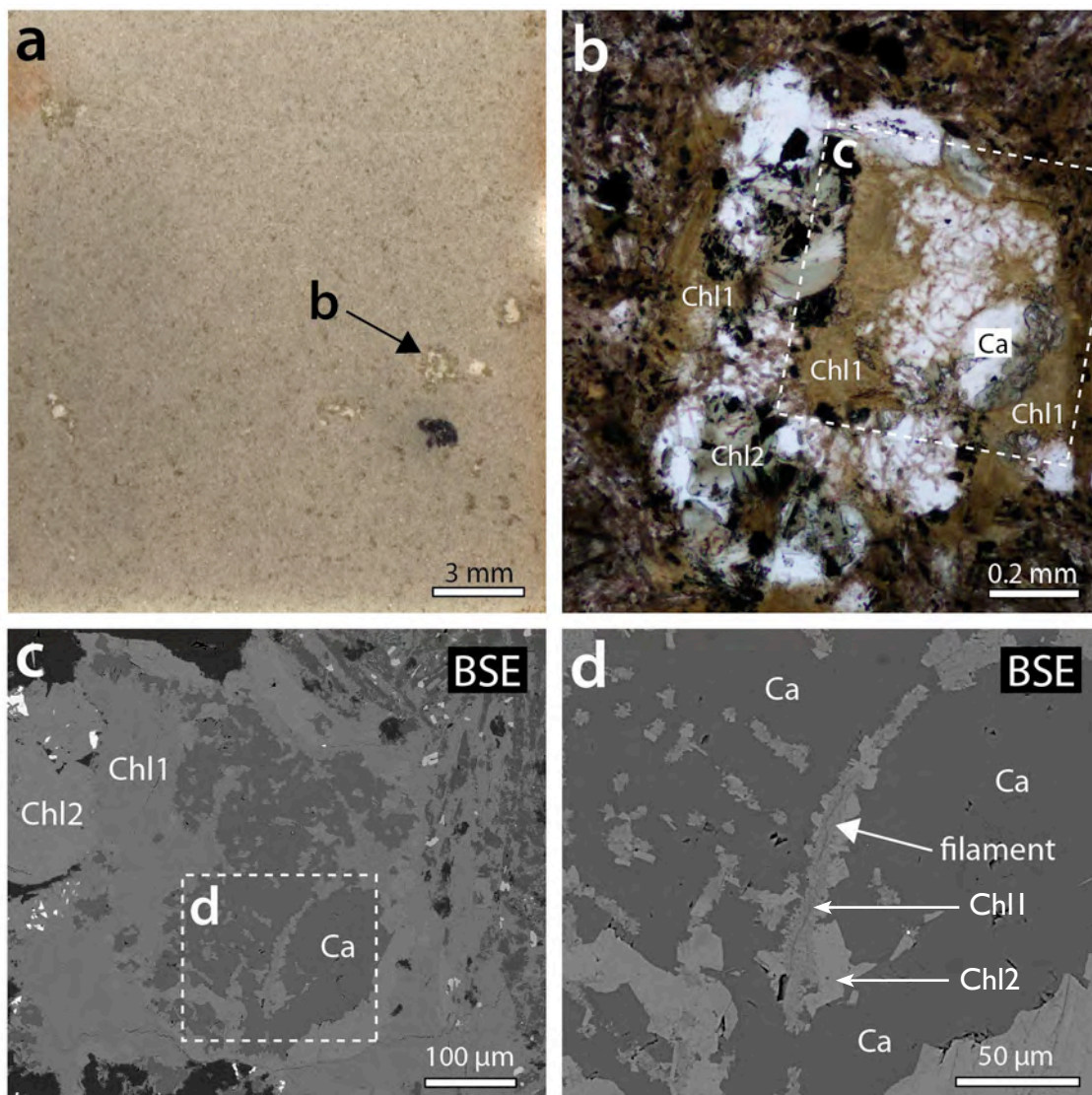


**Supplementary Figure 2 | Diagrams showing unprocessed Raman spectra from a calcite-filled cavity from the lower part of the Ongeluk Formation.** Spectrum (a) from the hyphae fossils demonstrates that they consist of chlorite, but no carbonaceous matter could be detected. A comparison can be made with spectrum (b) from the surrounding calcite. Chlorite bands (in Roman) are identified after data in Kleppe and Jephcoat<sup>26</sup> and calcite bands (in italics) after data in Downs<sup>27</sup>.

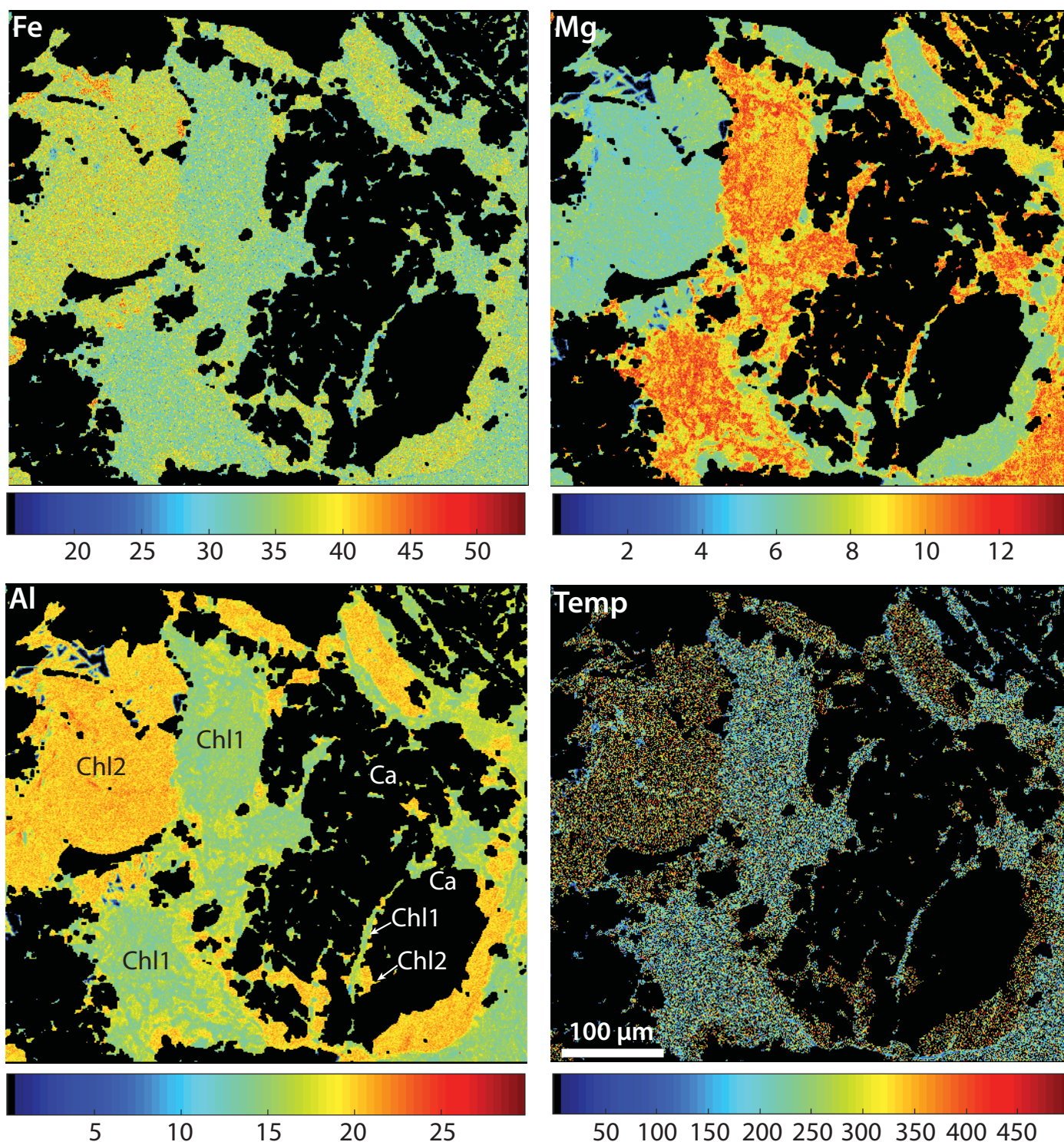


**Supplementary Figure 3 | Ongeluk vesicles with filamentous fossils, SRXTM surface/volume renderings of thin section. a, b, Vesicle showing density difference between marginal and central filament network and succes-**

**sive deposition of calcite (dark) and chlorite (light) cement; Swedish Museum of Natural History X6138. c, d, Vesicle with conspicuous brooms; X6139. Legend: Ca, Calcite; Chl1, Chlorite 1.**

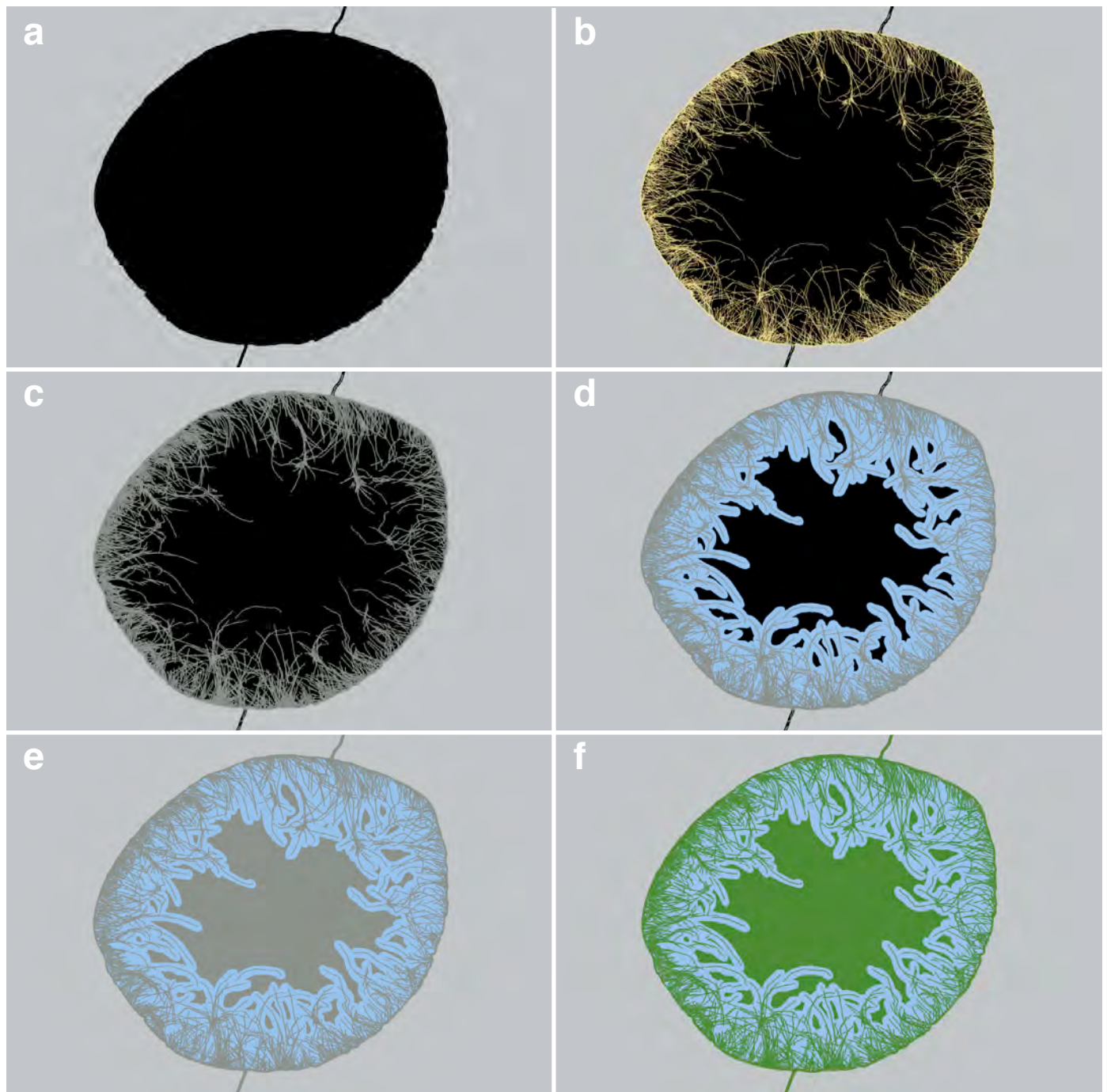


**Supplementary Figure 4 | Ongeluk vesicular basalt, petrographic thin section, ZBF061, Swedish Museum of Natural History X6409. a–b, Plane-polarized transmitted light; c–d, Back-scattered electron images. Image region the same as for WDS maps in Supplementary Fig. 5. Legend: Ca, calcite; Chl1, Chlorite 1; Chl2, Chlorite 2.**



**Supplementary Figure 5 | Quantitative element distribution maps** for FeO, MgO and Al<sub>2</sub>O<sub>3</sub> for chlorite from part of an amygdale in ZBF061, Swedish Museum of Natural History X6409. The maps were generated in XMapTools<sup>28</sup> from raw X-ray counts collected with wavelength dispersive spectrometers (WDS). A line of 25 point analyses (WDS) across Chlorite 1, and a separate line of 25 analyses across Chlorite 2, were used to calibrate the element maps (analysis points not shown). The temperature map (Temp)

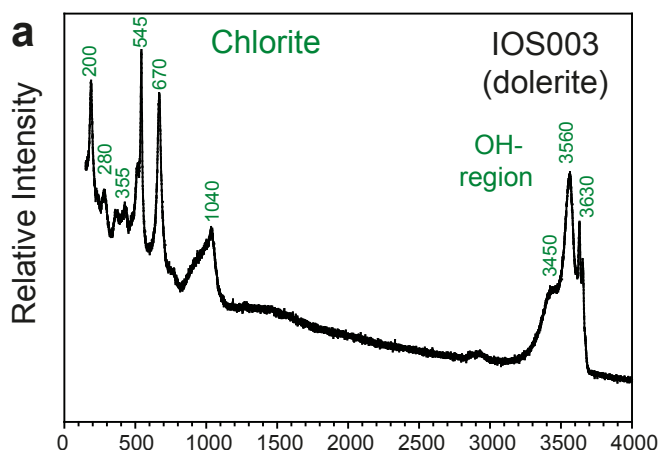
was generated in XMapTools from the element distribution maps, as well as those of SiO<sub>2</sub>, TiO<sub>2</sub>, CaO, K<sub>2</sub>O and Na<sub>2</sub>O, using a pixel by pixel calculation based on the Bourdelle et al.<sup>15</sup> geothermometer. The element maps show the distinct compositions of Chlorite 1 and Chlorite 2, which are reflected in the temperature map. A filamentous structure within calcite is composed of a central layer of Chlorite 1, but shows some growth of Chlorite 2 on its margins (see arrows). Legend: Ca, calcite; Chl1, Chlorite 1; Chl2, Chlorite 2.



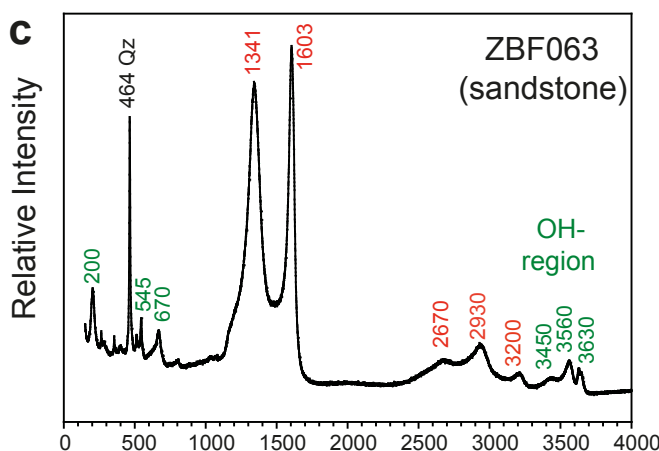
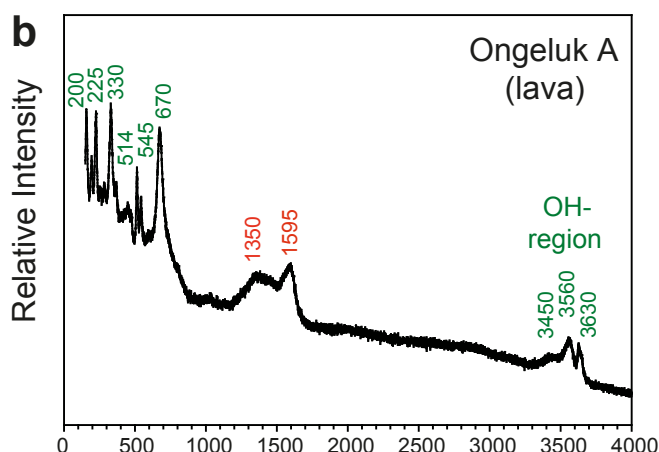
**Supplementary Figure 6 | Proposed fossilization sequence of filaments in Ongeluk vesicle.** **a**, Empty vesicle, connected to outside via a crack to allow inflow of water; **b**, Colonization of vesicle by mycelial organism; **c**, Mineraliza-

tion of filaments by smectite clay; **d**, Encrustation of filaments by calcite rims; **e**, Infilling of empty space with diagenetic clays; **f**, Metamorphic chloritization (Chlorite 1) of clay minerals in filaments and cavities.

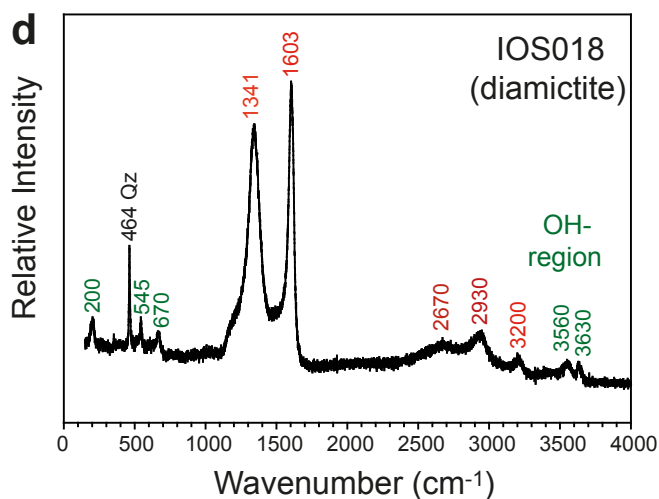
# DOLERITE DYKE



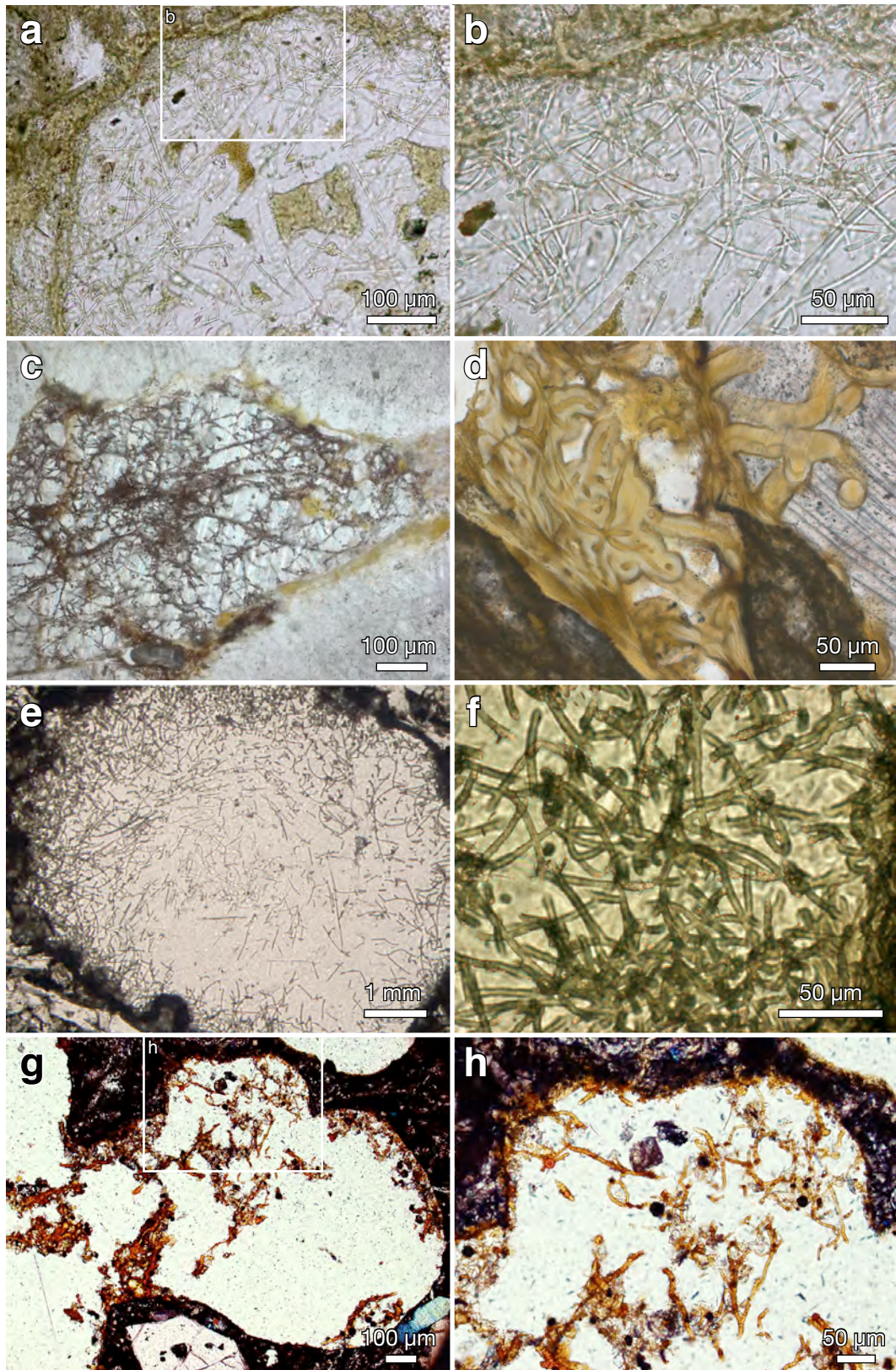
# ONGELUK FORMATION



# MAKGANYENE FORMATION



**Supplementary Figure 7 | Diagrams showing unprocessed Raman spectra** of samples from a stratigraphic sequence comprising (a) a dolerite immediately above the Ongeluk sample, (b) volcanic matrix in the lower part of the Ongeluk Formation, (c) a sandstone at the base of the Ongeluk Formation, and (d) a diamictite in the underlying Makganyene Formation. Chlorite bands (green) are identified after data in Kleppe and Jephcoat<sup>26</sup>, quartz (Qz) after data in Downs<sup>27</sup> and bands from carbonaceous material, CM (red), are identified after data in Rahl et al.<sup>18</sup>. The ordering of the CM structure is reflected by its Raman spectra and there is a correlation between the ~1350 and ~1600 cm<sup>-1</sup> bands (intensity, area, width) and maximum metamorphic temperature. The Raman spectra of CM in b–d can therefore be used as a geothermometer<sup>17,18</sup> and indicate metamorphic temperatures for the sedimentary base of the Ongeluk Formation (c) and the Makganyene Formation (d) of around 370°C and for the disordered CM from the Ongeluk Formation (b) of approximately 200±30°C.



**Supplementary Figure 8 | Comparative images of fossilized mycelia in vesicular volcanics of different ages. a, b,** Palaeoproterozoic Ongeluk Formation; Swedish Museum of Natural History X6130, same specimen as in Fig. 2b. **c, d,** Middle Devonian, Arnstein, Germany; images courtesy of J. Peckmann<sup>22</sup>. **e, f,** Eocene, Ocean Drilling Programme Site 1224, North Pacific; from Schumann et al. 2004<sup>21</sup>, fig. 1A, B, reprinted by permission of the publisher (Taylor & Francis Ltd, <http://www.tandfonline.com>). **g, h,** Quaternary, Vesteris Seamount, North Atlantic, Geoscience Museum of the University of Göttingen, Germany (GZG-PB.4041)<sup>29</sup>.

Supplementary Table 1. EDS spectra of Section IOS004.

IOS004	Am 1	Am 1	Am 1	Am 1	Am 2	Am 2	Am 2
	Chl 1	Chl 1	Chl 1	Chl 1	Chl 1	Chl 1	Chl 1
<b>Label</b>	<b>194</b>	<b>205</b>	<b>206</b>	<b>215</b>	<b>222</b>	<b>223</b>	<b>225</b>
SiO2	27.11	27.61	27.79	27.30	27.80	28.12	27.79
TiO2	0.00	0.00	0.00	0.00	0.00	0.00	0.00
Al2O3	15.76	14.84	14.55	14.57	14.75	14.86	14.70
Cr2O3	0.00	0.00	0.00	0.00	0.00	0.00	0.00
FeO	32.18	31.67	31.93	31.46	31.66	31.71	32.32
MnO	0.00	0.00	0.00	0.00	0.00	0.00	0.00
MgO	9.79	10.01	10.23	10.23	10.34	10.37	10.50
CaO	0.37	0.68	0.50	0.49	0.55	0.77	0.68
Na2O	0.12	0.00	0.00	0.00	0.00	0.00	0.00
K2O	0.00	0.00	0.00	0.00	0.00	0.00	0.00
<b>TOTAL</b>	<b>85.33</b>	<b>84.81</b>	<b>85.00</b>	<b>84.05</b>	<b>85.10</b>	<b>85.82</b>	<b>85.99</b>
<b>Cations/14 Ox</b>							
Si	3.06	3.13	3.15	3.12	3.14	3.14	3.12
Ti	0.00	0.00	0.00	0.00	0.00	0.00	0.00
Al	2.10	1.98	1.94	1.97	1.96	1.96	1.94
Cr	0.00	0.00	0.00	0.00	0.00	0.00	0.00
Fe2+	3.04	3.00	3.02	3.01	2.99	2.97	3.03
Mn	0.00	0.00	0.00	0.00	0.00	0.00	0.00
Mg	1.65	1.69	1.73	1.75	1.74	1.73	1.76
Ca	0.05	0.08	0.06	0.06	0.07	0.09	0.08
Na	0.03	0.00	0.00	0.00	0.00	0.00	0.00
K	0.00	0.00	0.00	0.00	0.00	0.00	0.00
<b>TOTAL</b>	<b>9.91</b>	<b>9.88</b>	<b>9.89</b>	<b>9.90</b>	<b>9.89</b>	<b>9.88</b>	<b>9.92</b>
ToC	218	198	199	214	201	199	234

Supplementary Table 2. EDS spectra of Section ZBF061.

Label	Am 1				Am 2				Am 3				Am 3				Am 3				Gmass																																																																																																																																																																																																																																																																																																																																																																																																																																																																																																																																																																																																																																																																																																																																																																																																																																																																														
	Chl 1	Chl 1	Chl 1	Chl 1	Chl 1	Chl 1	Chl 1	Chl 1	Chl 1	Chl 1	Chl 1	Chl 1	Chl 1	Chl 1	Chl 1	Chl 1	Chl 1	Chl 2	Chl 2	Chl 2	Chl 2	Chl 2	Chl 2	Chl 2	Chl 2	Chl 2	Chl 2	Chl 2	Chl 2	Chl 2	Chl 2	Chl 2	Chl 2	Chl 2	Chl 2	Chl 2	Chl 2	Chl 2	Chl 2	Chl 2	Chl 2	Chl 2	Chl 2	Chl 2	Chl 2	Chl 2	Chl 2	Chl 2	Chl 2	Chl 2	Chl 2	Chl 2	Chl 2	Chl 2	Chl 2	Chl 2	Chl 2	Chl 2	Chl 2	Chl 2	Chl 2	Chl 2	Chl 2	Chl 2	Chl 2	Chl 2	Chl 2	Chl 2	Chl 2	Chl 2	Chl 2	Chl 2	Chl 2	Chl 2	Chl 2	Chl 2	Chl 2	Chl 2	Chl 2	Chl 2	Chl 2	Chl 2	Chl 2	Chl 2	Chl 2	Chl 2	Chl 2	Chl 2	Chl 2	Chl 2	Chl 2	Chl 2	Chl 2	Chl 2	Chl 2	Chl 2	Chl 2	Chl 2	Chl 2	Chl 2	Chl 2	Chl 2	Chl 2	Chl 2	Chl 2	Chl 2	Chl 2	Chl 2	Chl 2	Chl 2	Chl 2	Chl 2	Chl 2	Chl 2	Chl 2	Chl 2	Chl 2	Chl 2	Chl 2	Chl 2	Chl 2	Chl 2	Chl 2	Chl 2	Chl 2	Chl 2	Chl 2	Chl 2	Chl 2	Chl 2	Chl 2	Chl 2	Chl 2	Chl 2	Chl 2	Chl 2	Chl 2	Chl 2	Chl 2	Chl 2	Chl 2	Chl 2	Chl 2	Chl 2	Chl 2	Chl 2	Chl 2	Chl 2	Chl 2	Chl 2	Chl 2	Chl 2	Chl 2	Chl 2	Chl 2	Chl 2	Chl 2	Chl 2	Chl 2	Chl 2	Chl 2	Chl 2	Chl 2	Chl 2	Chl 2	Chl 2	Chl 2	Chl 2	Chl 2	Chl 2	Chl 2	Chl 2	Chl 2	Chl 2	Chl 2	Chl 2	Chl 2	Chl 2	Chl 2	Chl 2	Chl 2	Chl 2	Chl 2	Chl 2	Chl 2	Chl 2	Chl 2	Chl 2	Chl 2	Chl 2	Chl 2	Chl 2	Chl 2	Chl 2	Chl 2	Chl 2	Chl 2	Chl 2	Chl 2	Chl 2	Chl 2	Chl 2	Chl 2	Chl 2	Chl 2	Chl 2	Chl 2	Chl 2	Chl 2	Chl 2	Chl 2	Chl 2	Chl 2	Chl 2	Chl 2	Chl 2	Chl 2	Chl 2	Chl 2	Chl 2	Chl 2	Chl 2	Chl 2	Chl 2	Chl 2	Chl 2	Chl 2	Chl 2	Chl 2	Chl 2	Chl 2	Chl 2	Chl 2	Chl 2	Chl 2	Chl 2	Chl 2	Chl 2	Chl 2	Chl 2	Chl 2	Chl 2	Chl 2	Chl 2	Chl 2	Chl 2	Chl 2	Chl 2	Chl 2	Chl 2	Chl 2	Chl 2	Chl 2	Chl 2	Chl 2	Chl 2	Chl 2	Chl 2	Chl 2	Chl 2	Chl 2	Chl 2	Chl 2	Chl 2	Chl 2	Chl 2	Chl 2	Chl 2	Chl 2	Chl 2	Chl 2	Chl 2	Chl 2	Chl 2	Chl 2	Chl 2	Chl 2	Chl 2	Chl 2	Chl 2	Chl 2	Chl 2	Chl 2	Chl 2	Chl 2	Chl 2	Chl 2	Chl 2	Chl 2	Chl 2	Chl 2	Chl 2	Chl 2	Chl 2	Chl 2	Chl 2	Chl 2	Chl 2	Chl 2	Chl 2	Chl 2	Chl 2	Chl 2	Chl 2	Chl 2	Chl 2	Chl 2	Chl 2	Chl 2	Chl 2	Chl 2	Chl 2	Chl 2	Chl 2	Chl 2	Chl 2	Chl 2	Chl 2	Chl 2	Chl 2	Chl 2	Chl 2	Chl 2	Chl 2	Chl 2	Chl 2	Chl 2	Chl 2	Chl 2	Chl 2	Chl 2	Chl 2	Chl 2	Chl 2	Chl 2	Chl 2	Chl 2	Chl 2	Chl 2	Chl 2	Chl 2	Chl 2	Chl 2	Chl 2	Chl 2	Chl 2	Chl 2	Chl 2	Chl 2	Chl 2	Chl 2	Chl 2	Chl 2	Chl 2	Chl 2	Chl 2	Chl 2	Chl 2	Chl 2	Chl 2	Chl 2	Chl 2	Chl 2	Chl 2	Chl 2	Chl 2	Chl 2	Chl 2	Chl 2	Chl 2	Chl 2	Chl 2	Chl 2	Chl 2	Chl 2	Chl 2	Chl 2	Chl 2	Chl 2	Chl 2	Chl 2	Chl 2	Chl 2	Chl 2	Chl 2	Chl 2	Chl 2	Chl 2	Chl 2	Chl 2	Chl 2	Chl 2	Chl 2	Chl 2	Chl 2	Chl 2	Chl 2	Chl 2	Chl 2	Chl 2	Chl 2	Chl 2	Chl 2	Chl 2	Chl 2	Chl 2	Chl 2	Chl 2	Chl 2	Chl 2	Chl 2	Chl 2	Chl 2	Chl 2	Chl 2	Chl 2	Chl 2	Chl 2	Chl 2	Chl 2	Chl 2	Chl 2	Chl 2	Chl 2	Chl 2	Chl 2	Chl 2	Chl 2	Chl 2	Chl 2	Chl 2	Chl 2	Chl 2	Chl 2	Chl 2	Chl 2	Chl 2	Chl 2	Chl 2	Chl 2	Chl 2	Chl 2	Chl 2	Chl 2	Chl 2	Chl 2	Chl 2	Chl 2	Chl 2	Chl 2	Chl 2	Chl 2	Chl 2	Chl 2	Chl 2	Chl 2	Chl 2	Chl 2	Chl 2	Chl 2	Chl 2	Chl 2	Chl 2	Chl 2	Chl 2	Chl 2	Chl 2	Chl 2	Chl 2	Chl 2	Chl 2	Chl 2	Chl 2	Chl 2	Chl 2	Chl 2	Chl 2	Chl 2	Chl 2	Chl 2	Chl 2	Chl 2	Chl 2	Chl 2	Chl 2	Chl 2	Chl 2	Chl 2	Chl 2	Chl 2	Chl 2	Chl 2	Chl 2	Chl 2	Chl 2	Chl 2	Chl 2	Chl 2	Chl 2	Chl 2	Chl 2	Chl 2	Chl 2	Chl 2	Chl 2	Chl 2	Chl 2	Chl 2	Chl 2	Chl 2	Chl 2	Chl 2	Chl 2	Chl 2	Chl 2	Chl 2	Chl 2	Chl 2	Chl 2	Chl 2	Chl 2	Chl 2	Chl 2	Chl 2	Chl 2	Chl 2	Chl 2	Chl 2	Chl 2	Chl 2	Chl 2	Chl 2	Chl 2	Chl 2	Chl 2	Chl 2	Chl 2	Chl 2	Chl 2	Chl 2	Chl 2	Chl 2	Chl 2	Chl 2	Chl 2	Chl 2	Chl 2	Chl 2	Chl 2	Chl 2	Chl 2	Chl 2	Chl 2	Chl 2	Chl 2	Chl 2	Chl 2	Chl 2	Chl 2	Chl 2	Chl 2	Chl 2	Chl 2	Chl 2	Chl 2	Chl 2	Chl 2	Chl 2	Chl 2	Chl 2	Chl 2	Chl 2	Chl 2	Chl 2	Chl 2	Chl 2	Chl 2	Chl 2	Chl 2	Chl 2	Chl 2	Chl 2	Chl 2	Chl 2	Chl 2	Chl 2	Chl 2	Chl 2	Chl 2	Chl 2	Chl 2	Chl 2	Chl 2	Chl 2	Chl 2	Chl 2	Chl 2	Chl 2	Chl 2	Chl 2	Chl 2	Chl 2	Chl 2	Chl 2	Chl 2	Chl 2	Chl 2	Chl 2	Chl 2	Chl 2	Chl 2	Chl 2	Chl 2	Chl 2	Chl 2	Chl 2	Chl 2	Chl 2	Chl 2	Chl 2	Chl 2	Chl 2	Chl 2	Chl 2	Chl 2	Chl 2	Chl 2	Chl 2	Chl 2	Chl 2	Chl 2	Chl 2	Chl 2	Chl 2	Chl 2	Chl 2	Chl 2	Chl 2	Chl 2	Chl 2	Chl 2	Chl 2	Chl 2	Chl 2	Chl 2	Chl 2	Chl 2	Chl 2	Chl 2	Chl 2	Chl 2	Chl 2	Chl 2	Chl 2	Chl 2	Chl 2	Chl 2	Chl 2	Chl 2	Chl 2	Chl 2	Chl 2	Chl 2	Chl 2	Chl 2	Chl 2	Chl 2	Chl 2	Chl 2	Chl 2	Chl 2	Chl 2	Chl 2	Chl 2	Chl 2	Chl 2	Chl 2	Chl 2	Chl 2	Chl 2	Chl 2	Chl 2	Chl 2	Chl 2	Chl 2	Chl 2	Chl 2	Chl 2	Chl 2	Chl 2	Chl 2	Chl 2	Chl 2	Chl 2	Chl 2	Chl 2	Chl 2	Chl 2	Chl 2	Chl 2	Chl 2	Chl 2	Chl 2	Chl 2	Chl 2	Chl 2	Chl 2	Chl 2	Chl 2	Chl 2	Chl 2	Chl 2	Chl 2	Chl 2	Chl 2	Chl 2	Chl 2	Chl 2	Chl 2	Chl 2	Chl 2	Chl 2	Chl 2	Chl 2	Chl 2	Chl 2	Chl 2	Chl 2	Chl 2	Chl 2	Chl 2	Chl 2	Chl 2	Chl 2	Chl 2	Chl 2	Chl 2	Chl 2	Chl 2	Chl 2	Chl 2	Chl 2	Chl 2	Chl 2	Chl 2	Chl 2	Chl 2	Chl 2	Chl 2	Chl 2	Chl 2	Chl 2	Chl 2	Chl 2	Chl 2	Chl 2	Chl 2	Chl 2	Chl 2	Chl 2	Chl 2	Chl 2	Chl 2	Chl 2	Chl 2	Chl 2	Chl 2	Chl 2	Chl 2	Chl 2	Chl 2	Chl 2	Chl 2	Chl 2	Chl 2	Chl 2	Chl 2	Chl 2	Chl 2	Chl 2	Chl 2	Chl 2	Chl 2	Chl 2	Chl 2	Chl 2	Chl 2	Chl 2	Chl 2	Chl 2	Chl 2	Chl 2	Chl 2	Chl 2	Chl 2	Chl 2	Chl 2	Chl 2	Chl 2	Chl 2	Chl 2	Chl 2	Chl 2	Chl 2	Chl 2	Chl 2	Chl 2	Chl 2	Chl 2	Chl 2	Chl 2	Chl 2	Chl 2	Chl 2	Chl 2	Chl 2	Chl 2	Chl 2	Chl 2	Chl 2	Chl 2	Chl 2	Chl 2	Chl 2	Chl 2	Chl 2	Chl 2	Chl 2	Chl 2	Chl 2	Chl 2	Chl 2	Chl 2	Chl 2	Chl 2	Chl 2	Chl 2	Chl 2	Chl 2	Chl 2	Chl 2	Chl 2	Chl 2	Chl 2	Chl 2	Chl 2	Chl 2	Chl 2	Chl 2	Chl 2	Chl 2	Chl 2	Chl 2	Chl 2	Chl 2	Chl 2	Chl 2	Chl 2	Chl 2	Chl 2	Chl 2	Chl 2	Chl 2	Chl 2	Chl 2	Chl 2	Chl 2

T oC (B) Temperature calculated per Bourdelle et al. 2013

T oC (L) Temperature calculated per Lanari et al. 2014

n.a. Temperature calculation not applicable (outside calibration range)

Supplementary Table 3. WDS spectra of Section ZBF061.

Spectrum	Ch1	Ch1	Ch1	Ch1	Ch1	Ch1	Ch1	Ch1	Ch1	Ch1	Ch1	Ch1	Ch1	Ch1	Ch1	Ch1	Ch1	Ch1	Ch1	Ch1	Ch1	Ch1	Ch1
SiO2	24.29	26.95	27.24	29.30	28.83	28.10	28.68	29.05	28.05	28.22	27.08	28.88	29.80	29.77	29.41	29.31	29.74	29.10	28.38	29.53	29.63	29.30	24.29
TiO2	0.00	0.00	0.06	0.09	0.00	0.04	0.00	0.06	0.03	0.02	0.00	0.00	0.05	0.03	0.00	0.00	0.00	0.00	0.04	0.00	0.00	0.00	
Al2O3	20.03	18.05	17.35	13.90	13.93	16.20	14.51	13.68	15.30	16.67	16.23	14.17	13.51	12.88	14.43	14.97	14.96	14.95	15.06	13.57	13.65	13.22	20.03
Cr2O3	0.00	0.00	0.00	0.00	0.00	0.00	0.00	0.00	0.00	0.00	0.00	0.00	0.00	0.00	0.00	0.00	0.00	0.00	0.00	0.00	0.00	0.00	
FeO	36.08	35.90	34.85	33.39	33.61	33.46	32.66	33.52	32.86	34.85	34.77	32.97	33.55	32.19	33.28	33.18	34.05	32.72	32.94	32.04	31.67	32.01	
MnO	0.10	0.11	0.11	0.10	0.10	0.09	0.07	0.07	0.10	0.11	0.09	0.08	0.07	0.07	0.10	0.12	0.07	0.08	0.09	0.09	0.07	0.05	
MgO	6.93	8.51	8.81	11.19	10.81	9.85	11.00	11.50	9.99	9.52	9.19	10.87	11.74	12.24	11.15	10.82	11.18	10.26	10.26	11.83	11.38	12.17	
CaO	0.17	0.28	0.30	0.21	0.17	0.20	0.16	0.12	0.17	0.20	0.18	0.17	0.12	0.11	0.19	0.18	0.18	0.23	0.23	0.12	0.13	0.12	
Na2O	0.00	0.00	0.00	0.00	0.00	0.04	0.06	0.00	0.00	0.03	0.00	0.00	0.00	0.00	0.00	0.00	0.00	0.00	0.00	0.03	0.00	0.00	
K2O	0.00	0.02	0.00	0.00	0.00	0.00	0.04	0.00	0.04	0.05	0.00	0.02	0.04	0.04	0.00	0.04	0.00	0.04	0.02	0.00	0.02	0.00	
TOTAL	87.62	89.86	88.73	88.19	87.46	88.03	87.15	88.01	86.54	89.68	87.58	87.17	88.88	87.33	88.58	88.63	90.21	87.41	86.98	87.24	86.58	86.88	

14 OX																						
Si	2.93	2.98	2.98	3.20	3.18	3.08	3.16	3.18	3.12	3.05	3.01	3.19	3.23	3.26	3.19	3.17	3.17	3.19	3.14	3.24	3.26	3.23
Ti	0.00	0.00	0.00	0.01	0.00	0.00	0.00	0.00	0.00	0.00	0.00	0.00	0.00	0.00	0.00	0.00	0.00	0.00	0.00	0.00	0.00	0.00
Al	2.31	2.24	2.24	1.79	1.81	2.09	1.89	1.77	2.01	2.12	2.13	1.84	1.72	1.66	1.85	1.91	1.88	1.93	1.96	1.75	1.77	1.72
Cr	0.00	0.00	0.00	0.00	0.00	0.00	0.00	0.00	0.00	0.00	0.00	0.00	0.00	0.00	0.00	0.00	0.00	0.00	0.00	0.00	0.00	0.00
Fe	3.26	3.19	3.19	3.05	3.10	3.06	3.01	3.07	3.06	3.15	3.23	3.04	3.04	2.95	3.02	3.01	3.04	3.00	3.05	2.94	2.92	2.95
Mn	0.01	0.01	0.01	0.01	0.01	0.01	0.01	0.01	0.01	0.01	0.01	0.01	0.01	0.01	0.01	0.01	0.01	0.01	0.01	0.01	0.01	0.00
Mg	1.38	1.44	1.44	1.82	1.78	1.61	1.81	1.88	1.66	1.53	1.52	1.79	1.89	2.00	1.80	1.75	1.78	1.68	1.69	1.93	1.87	2.00
Ca	0.03	0.03	0.03	0.03	0.02	0.02	0.02	0.01	0.02	0.02	0.02	0.02	0.01	0.01	0.02	0.02	0.02	0.03	0.03	0.01	0.02	0.01
Na	0.00	0.00	0.00	0.00	0.00	0.01	0.01	0.01	0.00	0.00	0.00	0.00	0.00	0.00	0.00	0.00	0.00	0.00	0.00	0.00	0.00	0.00
K	0.00	0.00	0.00	0.00	0.00	0.01	0.00	0.00	0.01	0.01	0.00	0.00	0.00	0.01	0.00	0.01	0.00	0.01	0.00	0.00	0.00	0.00
TOTAL	9.92	9.90	9.90	9.91	9.88	9.88	9.90	9.93	9.88	9.90	9.93	9.89	9.91	9.91	9.89	9.87	9.89	9.84	9.88	9.89	9.85	9.91

T oC (Bourdelle)	270	238	238	211	216	205	206	247	196	219	265	198	213	200	194	185	199	166	195	189	160	214
T oC (Lanari) <sup>1</sup>	212	137	137																			

Spectrum	1	2	3	5	6	7	8	9	10	11	12	13	14	16	17	18	19	20	21	22	23	
SiO2	24.49	24.28	24.21	24.01	24.06	24.04	23.91	23.76	23.58	24.41	24.94	24.21	24.78	24.15	24.06	23.91	23.68	24.42	24.09	24.37	24.50	24.45
TiO2	0.03	0.06	0.03	0.00	0.00	0.05	0.06	0.03	0.00	0.05	0.00	0.00	0.04	0.06	0.05	0.03	0.00	0.00	0.00	0.06	0.00	0.00
Al2O3	19.89	19.71	19.80	19.94	19.96	20.06	20.38	20.08	19.61	19.96	20.14	19.61	20.04	19.95	19.91	19.44	19.29	19.75	20.09	19.55	19.87	20.83
Cr2O3	0.00	0.00	0.00	0.00	0.00	0.00	0.00	0.00	0.00	0.00	0.00	0.00	0.00	0.00	0.00	0.00	0.00	0.00	0.00	0.00	0.00	
FeO	36.05	36.43	36.64	36.70	37.05	36.80	36.33	36.87	33.54	34.84	33.20	35.68	36.50	36.08	36.36	36.62	35.22	36.82	36.00	36.07	35.60	35.76
MnO	0.15	0.12	0.12	0.11	0.13	0.11	0.11	0.09	0.14	0.08	0.14	0.13	0.13	0.09	0.11	0.10	0.11	0.11	0.11	0.11	0.07	0.08
MgO	7.19	7.14	6.79	6.64	6.74	6.72	6.57	6.50	6.10	6.70	6.60	6.85	6.93	7.23	6.49	6.73	6.84	6.92	6.75	7.02	7.07	6.80
CaO	0.00	0.00	0.00	0.00	0.00	0.00	0.00	0.00	0.00	0.00	0.00	0.00	0.00	0.00	0.00	0.00	0.00	0.00	0.00	0.00	0.00	
Na2O	0.00	0.00	0.03	0.00	0.00	0.00	0.00	0.00	0.03	0.00	0.00	0.00	0.00	0.00	0.03	0.00	0.00	0.00	0.00	0.00	0.00	
K2O	0.00	0.04	0.00	0.00	0.00	0.00	0.00	0.00	0.02	0.00	0.00	0.00	0.00	0.00	0.00	0.00	0.00	0.00	0.00	0.00	0.00	
TOTAL	87.81	87.81	87.63	87.42	87.96	87.77	87.36	87.33	83.03	86.05	85.03	86.48	88.44	87.56	87.01	86.86	85.15	88.02	87.04	87.21	87.15	87.94

14 OX																																																																																																																																																																																																																																																																																																																																																																																																																																																																																																																																																																																																																																																																																																																																																																																																																																																																																																																																																																																																																																																																																																																																																																																																																																																																																																																																																																																																																																						
-------	--	--	--	--	--	--	--	--	--	--	--	--	--	--	--	--	--	--	--	--	--	--	--	--	--	--	--	--	--	--	--	--	--	--	--	--	--	--	--	--	--	--	--	--	--	--	--	--	--	--	--	--	--	--	--	--	--	--	--	--	--	--	--	--	--	--	--	--	--	--	--	--	--	--	--	--	--	--	--	--	--	--	--	--	--	--	--	--	--	--	--	--	--	--	--	--	--	--	--	--	--	--	--	--	--	--	--	--	--	--	--	--	--	--	--	--	--	--	--	--	--	--	--	--	--	--	--	--	--	--	--	--	--	--	--	--	--	--	--	--	--	--	--	--	--	--	--	--	--	--	--	--	--	--	--	--	--	--	--	--	--	--	--	--	--	--	--	--	--	--	--	--	--	--	--	--	--	--	--	--	--	--	--	--	--	--	--	--	--	--	--	--	--	--	--	--	--	--	--	--	--	--	--	--	--	--	--	--	--	--	--	--	--	--	--	--	--	--	--	--	--	--	--	--	--	--	--	--	--	--	--	--	--	--	--	--	--	--	--	--	--	--	--	--	--	--	--	--	--	--	--	--	--	--	--	--	--	--	--	--	--	--	--	--	--	--	--	--	--	--	--	--	--	--	--	--	--	--	--	--	--	--	--	--	--	--	--	--	--	--	--	--	--	--	--	--	--	--	--	--	--	--	--	--	--	--	--	--	--	--	--	--	--	--	--	--	--	--	--	--	--	--	--	--	--	--	--	--	--	--	--	--	--	--	--	--	--	--	--	--	--	--	--	--	--	--	--	--	--	--	--	--	--	--	--	--	--	--	--	--	--	--	--	--	--	--	--	--	--	--	--	--	--	--	--	--	--	--	--	--	--	--	--	--	--	--	--	--	--	--	--	--	--	--	--	--	--	--	--	--	--	--	--	--	--	--	--	--	--	--	--	--	--	--	--	--	--	--	--	--	--	--	--	--	--	--	--	--	--	--	--	--	--	--	--	--	--	--	--	--	--	--	--	--	--	--	--	--	--	--	--	--	--	--	--	--	--	--	--	--	--	--	--	--	--	--	--	--	--	--	--	--	--	--	--	--	--	--	--	--	--	--	--	--	--	--	--	--	--	--	--	--	--	--	--	--	--	--	--	--	--	--	--	--	--	--	--	--	--	--	--	--	--	--	--	--	--	--	--	--	--	--	--	--	--	--	--	--	--	--	--	--	--	--	--	--	--	--	--	--	--	--	--	--	--	--	--	--	--	--	--	--	--	--	--	--	--	--	--	--	--	--	--	--	--	--	--	--	--	--	--	--	--	--	--	--	--	--	--	--	--	--	--	--	--	--	--	--	--	--	--	--	--	--	--	--	--	--	--	--	--	--	--	--	--	--	--	--	--	--	--	--	--	--	--	--	--	--	--	--	--	--	--	--	--	--	--	--	--	--	--	--	--	--	--	--	--	--	--	--	--	--	--	--	--	--	--	--	--	--	--	--	--	--	--	--	--	--	--	--	--	--	--	--	--	--	--	--	--	--	--	--	--	--	--	--	--	--	--	--	--	--	--	--	--	--	--	--	--	--	--	--	--	--	--	--	--	--	--	--	--	--	--	--	--	--	--	--	--	--	--	--	--	--	--	--	--	--	--	--	--	--	--	--	--	--	--	--	--	--	--	--	--	--	--	--	--	--	--	--	--	--	--	--	--	--	--	--	--	--	--	--	--	--	--	--	--	--	--	--	--	--	--	--	--	--	--	--	--	--	--	--	--	--	--	--	--	--	--	--	--	--	--	--	--	--	--	--	--	--	--	--	--	--	--	--	--	--	--	--	--	--	--	--	--	--	--	--	--	--	--	--	--	--	--	--	--	--	--	--	--	--	--	--	--	--	--	--	--	--	--	--	--	--	--	--	--	--	--	--	--	--	--	--	--	--	--	--	--	--	--	--	--	--	--	--	--	--	--	--	--	--	--	--	--	--	--	--	--	--	--	--	--	--	--	--	--	--	--	--	--	--	--	--	--	--	--	--	--	--	--	--	--	--	--	--	--	--	--	--	--	--	--	--	--	--	--	--	--	--	--	--	--	--	--	--	--	--	--	--	--	--	--	--	--	--	--	--	--	--	--	--	--	--	--	--	--	--	--	--	--	--	--	--	--	--	--	--	--	--	--	--	--	--	--	--	--	--	--	--	--	--	--	--	--	--	--	--	--	--	--	--	--	--	--	--	--	--	--	--	--	--	--	--	--	--	--	--	--	--	--	--	--	--	--	--	--	--	--	--	--	--	--	--	--	--	--	--	--	--	--	--	--	--	--	--	--	--	--	--	--	--	--	--	--	--	--	--	--	--	--	--	--	--	--	--	--	--	--	--	--	--	--	--	--	--	--	--	--	--	--	--	--	--	--	--	--	--	--	--	--	--	--	--	--	--	--	--	--	--	--	--	--	--	--	--	--	--	--	--	--	--	--	--	--	--	--	--	--	--	--	--	--	--	--	--	--	--	--	--	--	--	--	--	--	--	--	--	--	--	--	--	--	--	--	--	--	--	--	--	--	--	--	--	--	--	--	--	--	--	--	--	--	--	--	--	--	--	--	--	--	--	--	--	--	--	--	--	--	--	--	--	--	--	--	--	--	--	--	--	--	--	--	--	--	--	--	--	--	--	--	--	--	--	--	--	--	--	--	--	--	--	--	--	--	--	--	--	--	--	--	--	--	--	--	--	--	--	--	--	--	--	--	--	--	--	--	--	--	--	--	--	--	--	--	--	--	--	--	--	--	--	--	--	--	--	--	--	--	--	--	--	--	--	--	--	--	--	--	--	--	--	--	--	--	--	--	--	--	--	--	--	--	--	--	--	--	--	--	--	--	--	--	--	--	--	--	--	--	--	--	--	--	--	--	--	--	--	--	--	--	--	--	--	--	--	--	--	--	--	--	--	--	--	--	--	--	--	--	--	--	--	--	--	--	--	--	--	--	--	--	--	--	--	--	--	--	--	--	--	--	--	--	--	--	--	--	--	--	--	--	--	--	--	--	--	--	--	--	--	--	--	--	--	--	--	--	--	--	--	--	--	--	--	--	--	--	--	--	--	--	--	--	--	--	--	--	--	--	--	--	--	--	--	--	--	--	--	--	--	--	--

T oC (Bourdelle) <sup>2</sup>	384	505	433	440	530	486	402	509	244	268	200	342	336	485	373	530	389	426	364	387	322	304
T oC (Lanari)	329	413	376	379	442	389	340	416	229	238	181	303	290	388	327	422	340	365	323	320	290	278

## References

- Grobler, N. J. & Botha, B. J. V. Pillow-lavas and hyaloclastite in the Ongeluk Andesite Formation in a road-cutting west of Griquatown, South Africa. *Trans Geol Soc S Afr* **79**, 53–57 (1976).
- Cornell, D. H., Schütte, S. S. & Eglington, B. L. The Ongeluk basaltic andesite formation in Griqualand West, South Africa: submarine alteration in a 2222 Ma Proterozoic sea. *Precambrian Res.* **79**, 101–123 (1996).
- Miyano, T. & Beukes, N. J. Physicochemical environments for the formation of quartz-free manganese oxide ores from the early Proterozoic Hotazel Formation, Kalahari manganese field, South Africa. *Economic Geology* **82**, 706–718 (1987).
- Gutzmer, J. et al. Ancient sub-seafloor alteration of basaltic andesites of the Ongeluk Formation, South Africa: implications for the chemistry of Paleoproterozoic seawater. *Chemical Geology* **201**, 37–53 (2003).
- Bau, M., Romer, R. L., Lüders, V. & Beukes, N. J. Pb, O, and C isotopes in silicified Mooidraai dolomite (Transvaal Supergroup, South Africa): implications for the composition of Paleoproterozoic seawater and “dating” the increase of oxygen in the Precambrian atmosphere. *Earth Planet Sci Lett* **174**, 43–57 (1999).
- Fairey, B., Tsikos, H., Corfu, F. & Polteau, S. U–Pb systematics in carbonates of the Postmasburg Group, Transvaal Supergroup, South Africa: Primary versus metasomatic controls. *Precambrian Res.* **231**, 194–205 (2013).
- Gumsley, A. et al. The timing and tempo of the Great Oxidation Event. *Proc. Natl. Acad. Sci. USA* **online**, 6 pp., doi:10.1073/pnas.1608824114 (2017).
- Rasmussen, B., Fletcher, I. R., Muhling, J. R., Mueller, A. G. & Hall, G. C. Bushveld-aged fluid flow, peak metamorphism, and gold mobilization in the Witwatersrand basin, South Africa: Constraints from in situ SHRIMP U–Pb dating of monazite and xenotime. *Geology* **35**, 931–934 (2007).
- Rasmussen, B., Bekker, A. & Fletcher, I. R. Correlation of Paleoproterozoic glaciations based on U–Pb zircon ages for tuff beds in the Transvaal and Huronian Supergroups. *Earth Planet Sci Lett* **382**, 173–180 (2013).
- Evans, D. A. D., Gutzmer, J., N. J. Beukes & Kirschvink, J. L. Paleomagnetic constraints on ages of mineralization in the Kalahari Manganese Field, South Africa. *Economic Geology* **96**, 621–631 (2001).
- Macfarlane, A. W. & Holland, H. D. The timing of alkali metasomatism in paleosols. *Canadian Mineralogist* **29**, 1043–1050 (1991).
- Phillips, W. J. Interpretation of crystalline spheroidal structures in igneous rocks. *Lithos* **6**, 235–244 (1973).
- Fowler, A. D., Berger, B., Shore, M., Jones, M. I. & Ropchan, J. Supercooled rocks: development and significance of varioles, spherulites, dendrites and spinifex in Archaean volcanic rocks, Abitibi Greenstone belt, Canada. *Precambrian Res.* **115**, 311–328 (2002).
- Sandstå, N. R., Robins, B., Furnes, H. & de Wit, M. The origin of large varioles in flow-banded pillow lava from the Hoogenoeg Complex, Barberton Greenstone Belt, South Africa. *Contributions to Mineralogy and Petrology* **162**, 365–377 (2011).
- Bourdelle, F., Parra, T., Chopin, C. & Beyssac, O. A new chlorite geothermometer for diagenetic to low-grade metamorphic conditions. *Contributions to Mineralogy and Petrology* **165**, 723–735 (2013).
- Lanari, P., Wagner, T. & Vidal, O. A thermodynamic model for di-trioctahedral chlorite from experimental and natural data in the system  $\text{MgO-FeO-Al}_2\text{O}_3\text{-SiO}_2\text{-H}_2\text{O}$ : applications to P–T sections and geothermometry. *Contributions to Mineralogy and Petrology* **167**, 19 pp., doi:10.1007/s00410-014-0968-8 (2014).
- Beyssac, O., Goffé, B., Chopin, C. & Rouzaud, J. N. Raman spectra of carbonaceous material in metasediments: a new geothermometer. *Journal of Metamorphic Geology* **20**, 859–871 (2002).
- Rahl, J. M., Anderson, K. M., Brandon, M. T. & Fassoulas, C. Raman spectroscopic carbonaceous material thermometry of low-grade metamorphic rocks: Calibration and application to tectonic exhumation in Crete, Greece. *Earth Planet Sci Lett* **240**, 339–354 (2005).
- McCloughlin, N., Staudigel, H., Furnes, H., Eickmann, B. & Ivarsson, M. Mechanisms of microtunneling in rock substrates: distinguishing endolithic biosignatures from abiotic microtunnels. *Geobiology* **8**, 245–255 (2010).
- Wacey, D. in *Early Life on Earth. A Practical Guide. Topics in Geobiology* **31** (ed David Wacey) 47–53 (Springer, 2009).
- Schumann, G., Manz, W., Reitner, J. & Lustrino, M. Ancient fungal life in North Pacific Eocene oceanic crust. *Geomicrobiol. J.* **21**, 241–246 (2004).
- Peckmann, J., Bach, W., Behrens, K. & Reitner, J. Putative cryptoendolithic life in Devonian pillow basalt, Rheinisches Schiefergebirge, Germany. *Geobiology* **6**, 125–135 (2008).
- Ivarsson, M., Bengtson, S., Skogby, H., Belivanova, V. & Marone, F. Fungal colonies in open fractures of subseafloor basalt. *Geo-Mar. Lett.* **33**, 233–243 (2013).
- Staudigel, H., Hart, S. R. & Richardson, S. H. Alteration of the oceanic crust: processes and timing. *Earth Planet Sci Lett* **52**, 311–327 (1981).
- Bourdelle, F. & Cathelineau, M. Low-temperature chlorite geothermometry: a graphical representation based on a T–Si–R<sup>2+</sup> diagram. *European Journal of Mineralogy* **27**, 617–626 (2015).
- Kleppe, A. K. & Jephcoat, A. P. in *Earth’s Deep Water Cycle. Geophysical Monograph Series* **168** (eds Steven D. Jacobsen & Suzan Van Der Lee) 69–93 (2006).
- Downs, R. T. The RRUFF Project: an integrated study of the chemistry, crystallography, Raman and infrared spectroscopy of minerals. *Program and Abstracts of the 19th General Meeting of the International Mineralogical Association in Kobe, Japan*, O03–13 (2006).
- Lanari, P. et al. XMapTools: A MATLAB®-based program for electron microprobe X-ray image processing and geothermobarometry. *Comput Geosci* **62**, 227–240 (2014).
- Ivarsson, M. et al. Zygomycetes in vesicular basanites from Vesteris Seamount, Greenland Basin – a new type of cryptoendolithic fungi. *PLoS ONE* **10**, 16 pp., doi:10.1371/journal.pone.0133368 (2015).